AN ABSTRACT OF THE THESIS OF

JAMES KENT HANCOCK (Name of student) for the Ph. D. (Degree)

in Chemistry (Major) presented on October 23, 1969 (Date)

Title: ULTRASONIC DISPERSION IN GASEOUS ALLENE, AMMONIA, AND CARBON SUBOXIDE OBSERVED BY OPTICAL DIFFRACTION

Redacted for privacy

Abstract approved J. C. Decius

Experimental sound velocities in gaseous ammonia, allene, and carbon suboxide have been measured at high frequencies using the optical diffraction method. In this method, ultrasonic waves generated in the gas act as a pseudo-grating and diffract the light rays passing parallel through the cell. A small He-Ne gas laser is used as a light source and ultrasound waves are generated using quartz transducers of frequencies 0.56, 1.07, and 1.78 MHz.

The velocity of sound in ammonia has been measured from 1.0-14 MHz/atm with no detection of vibrational relaxation in this range. The experimental velocity for ammonia is $V_i^2 = (19.087 \pm 0.008) \times 10^4$ $m^2/sec^2$ at 300°K which agrees within 0.03% of the static value based on a realistic statistical thermodynamical evaluation of the heat capacity. The correction for gas imperfection in ammonia has been determined experimentally by plotting $V^2$ vs. pressure. The value obtained, $S = -151 \pm 5$ cc/mole at 297°K is

in excellent agreement with those available from independent sources.

Sound velocity measurements in allene extend from 0.3-33 MHz/atm with the lower 1/4 of the dispersion curve for vibrational relaxation covered. All of the vibrational degrees of freedom relax together with $\tau = 5.2$ ns at 300°K. The nonideality parameter has been determined experimentally and we find S = -292 ± 1 cc/mole at 298°K in good agreement with values based on virial data.

Carbon suboxide has been studied from 1.1-41 MHz/atm and has been found to be doubly dispersive with all of the vibrational specific heat with the exception of the lowest bend ($\nu_7$=63 $cm^{-1}$) relaxing at $\tau_1$ = 48 ns at 300°K. The nonideality correction in carbon suboxide is estimated to be S = -490 cc/mole at 300°K based on the best fit of experimental data, taken at two different crystal frequencies, to the theoretical dispersion curve. The high frequency relaxation could not be observed, but on the basis of our data we estimate $\tau_2 \leq 1$ ns. The subject of multiple relaxation is discussed in detail and includes a survey of gases known to exhibit this behavior.

The intensity distribution of the first order diffraction images produced in the optical diffraction method have been measured photoelectrically for a number of selected gases. Intensity asymmetry has been observed which may be due to the rapid acoustic absorption exhibited by gases undergoing vibrational relaxation. Intensity asymmetry can also result from nonzero alignment of the light rays with

the ultrasound field and it has not proved possible to satisfactorily distinguish between these two effects.

# Ultrasonic Dispersion in Gaseous Allene, Ammonia and Carbon Suboxide Observed by Optical Diffraction

by

James Kent Hancock

A THESIS

submitted to

Oregon State University

in partial fulfillment of
the requirements for the
degree of

Doctor of Philosophy

June 1970

APPROVED:

Redacted for privacy

Professor of Chemistry
in charge of major

Redacted for privacy

Chairman of Department of Chemistry

Redacted for privacy

Dean of Graduate School

Date thesis is presented October 23, 1969

Typed by Opal Grossnicklaus for James Kent Hancock

ACKNOWLEDGMENT

It is my pleasure to acknowledge the invaluable contributions Dr. J. C. Decius has made, not only in the course of directing this thesis study, but also in establishing my future research interests and goals.

Much credit should also be given to Dr. J. V. Martinez and Dr. J. G. Strauch, Jr. Their efforts led to the construction of the basic instrument used to obtain data in this study.

I wish to thank the Office of Naval Research for their financial support throughout the investigation.

To

Diane

TABLE OF CONTENTS

## LIST OF TABLES

## LIST OF FIGURES

# ULTRASONIC DISPERSION IN GASEOUS ALLENE, AMMONIA, AND CARBON SUBOXIDE OBSERVED BY OPTICAL DIFFRACTION

## INTRODUCTION

### (1.1) Vibrational Energy Transfer in Gases

Ultrasonic velocity measurements represent one of many different experimental techniques used to determine molecular rate constants in gases. In vibrational energy transfer, the rate constant is a relaxation time associated with the limiting step in a quantum exchange process between the vibrational energy levels in a molecule and its external degrees of freedom, translation and rotation. Vibrational energy levels are referred to as internal degrees of freedom as they are not as readily sensitive to rapid environmental temperature fluctuations as is found with the translational and rotational energy levels. Most molecules at room temperature require only a few self collisions for their translational and rotational degrees of freedom to readjust to an external temperature change, while the vibrational states may require anywhere from ten to ten million collisions.

Temperature equilibrium on the molecular scale is defined in terms of the Boltzmann equation which relates the average number of molecules distributed over its various energy states to the absolute temperature of the environment.

$$N_i = \frac{N}{Q} G_i \exp(-E_i/kT) \qquad (1)$$

In equation (1), $Q$ is the partition function, $N_i$ represents the average number of molecules in level i, of energy $E_i$, and degeneracy $G_i$, and $N$ is the total number of molecules. In as much as the energy of the $i^{th}$ level is the sum of energies corresponding to the electronic $E_i^{el}$, vibrational $E_i^{vib}$, rotational $E_i^{rot}$, and translational $E_i^{tr}$, and $G_i$ may be regarded as a product of the degeneracies of these different energies, we may (provided the Hamiltonian will factor) separate equation (1) into four independent equations.

$$\text{Electronic} \quad N_i^{el} = (N/Q^{el})\, G_i^{el} \exp(-E_i^{el}/kT^{el}) \qquad (2a)$$

$$\text{Vibration} \quad N_i^{vib} = (N/Q^{vib})\, G_i^{vib} \exp(-E_i^{vib}/kT^{vib}) \qquad (2b)$$

$$\text{Rotation} \quad N_i^{rot} = (N/Q^{rot})\, G_i^{rot} \exp(-E_i^{rot}/kT^{rot}) \qquad (2c)$$

$$\text{Translation} \quad N_i^{tr} = (N/Q^{tr})\, G_i^{tr} \exp(-E_i^{tr}/kT^{tr}) \qquad (2d)$$

Equations (2abcd) define an independent temperature corresponding to each degree of freedom and true thermal equilibrium occurs only when equation (2) is obeyed and $T^{el} = T^{vib} = T^{rot} = T^{tr}$. Energy transfer, then may be regarded as a study of the rate constants and mechanisms by which a molecular system maintains its thermodynamical energy equilibrium in the face of rapidly changing environmental conditions. That the same molecule can exist in Boltzmann equilibrium according to equation (2) and still possess different internal and external

temperatures is a consequence of the vastly different equilibrium rates each degree of freedom may possess for adjusting to external temperature changes. A vivid demonstration of this was provided by Millikan (70) who highly excited the vibrational energy levels in carbon monoxide using an open, flowing system to prevent vibrational deactivation on walls. With this technique he was able to maintain the vibrational temperature in carbon monoxide at 993° K while the translational and rotational temperatures remained at 286° K.

Herzfeld and Rice (38) have established the form of the relaxation equation which relates the momentary value of the internal energy $E^{vib}$, to the value it would have in equilibrium with the translational degrees of freedom at temperature $T^{tr}$. This relationship, valid for one degree of vibrational freedom, is shown in equation (3).

$$\frac{-dE^{vib}}{dt} = \frac{1}{\tau}[E^{vib} - E^{vib}(T^{tr})] \qquad (3)$$

where $\tau$ is the relaxation time (reciprocal rate constant) describing the equilibration process. As indicated in equation (3) a sudden change in translational temperature is followed by an exponential decay of vibrational energy to a new equilibrium temperature, where, after $\tau$ seconds the energy discrepancy $|E^{vib} - E^{vib}(T^{tr})|$ is 37% or $(1/e)$ of its original value. Since polyatomic molecules possess (3N-6) degrees of vibrational freedom [(3N-5) if linear] one would expect when equation (3) is generalized,

to observe (3N-6) relaxation times. This assumes that each oscillatory degree of freedom behaves independently of the others and the relaxation process is describable as a group of parallel reactions. Experimentally this has not been found to be the case. Only one relaxation time is usually observed indicating a series relaxation process. For most molecules the rates of intermolecular and intramolecular vibrational-vibrational energy transfer are much faster than the conversion of vibrational to translational or rotational energy. Because of this, the single relaxation time measured in polyatomic molecules is associated with the transfer of energy into and out of the vibrational level closest to the ground state of the molecule.

With a few exceptions, of which carbon monoxide is an example, in gases at moderate temperatures and pressures the overwhelming majority of quantum transitions which take place occur only during molecular collisions. Landau and Teller (56) have shown that in order for vibrational-translational energy exchange to occur, the collision duration should be of the same order of magnitude as the period of vibration of the oscillator. As a simple approximation, the probability for deactivation is proportional to

$$P_{10} = A \exp\left[(-\ell/v)/(1/4\pi^2\nu)\right] \qquad (4)$$

where $A$ is of the order of $10^3$ [see equation (21) later] and $v$ is the relative velocity of the colliding molecules, $\nu$ is the frequency of the vibration in cycles per second and $\ell$ is the interaction

distance during which the bulk of the kinetic energy of the collision is converted into potential energy of interaction. Exponential repulsion due to the overlap between closed shell orbitals normally leads to potentials where $\ell$ is approximately 0.2 Å (63, 101). Molecular collisions occur over a wide range of velocities and only the fastest of these encounters have sufficient velocity, according to equation (4), to yield an appreciable probability of transition. Since the number of molecules with high velocity decreases strongly with increasing v, the two effects tend to cancel and it is possible to estimate the velocity for which a transition is most likely to occur. For a diatomic molecule with a vibrational frequency of 1000 $cm^{-1}$ and reduced mass 20 this velocity is $2 \times 10^5$ cm/sec [see equation (27)].

Substituting the values of our hypothetical gas into equation (4) provides an upper limit on the probability of vibrational energy transfer. The results show $P_{10} \approx 10^{-3}$, or under optimum conditions, 1000 collisions are needed per vibrational deactivation. The velocity used in our calculation is about a factor of five faster than the average relative velocity and because of this very few collisions occur with sufficient kinetic energy to cause a transition. The overall transition probability when summed over all interactions is, therefore, expected to be substantially smaller than the most efficient value calculated here.

In discussing vibrational energy transfer it has been implied

that conversion of vibrational to translational energy can occur only in those brief moments during which a molecule undergoes a collision. Between collisions the molecule remains fixed in the quantum state established during the preceeding encounter. No one molecule in isolation can exchange a vibrational quantum with its external degrees of freedom without violating the laws of conservation of momentum. Molecules can, however, lose one quantum of vibrational energy at any time by photon emission. The probability of radiative decay is directly related to the Einstein coefficient for spontaneous emission. Since radiative losses are independent of pressure and the frequency of molecular collisions varies directly with pressure, we can expect to reach a crossing point, as the pressure is lowered, where radiative emission can no longer be ignored. Calculations by Lukasik (60) indicate this point is reached at about one micron pressure and then only for the higher lying vibrational levels which possess strongly allowed electric dipole transitions.

A more important effect in influencing vibrational deactivation at low pressures is the degradation of energy in wall collisions. Little is known regarding such processes, but there is some indication that for simple polyatomic molecules wall collisions are very effective, requiring only one to ten collisions per deactivation (46, 51). The exact pressure at which wall effects become important depends on the cell dimensions as well as the vibrational relaxation time of

the gas being studied. Javan and his coworkers (51) in studying vibrational fluorescence from the 00°1 level in $CO_2$ found wall effects became important below 50 microns in a cell 2.5 cm in diameter and below 400 microns in a cell 0.8 cm in diameter. Since the majority of investigations occur at higher pressures and in larger systems than discussed above, the assumptions regarding molecular collisions as the sole source of energy transfer appear valid.

## (1.2) Experimental Methods in Vibrational Relaxation

Although many ingenious techniques have been devised to measure energy transfer processes, each in its simplest form may be explained using the separated Boltzmann equations shown in equations (2abcd). By supplying either kinetic energy or energy of a specific wavelength it is possible to selectively alter, momentarily, the energy levels of one of the four degrees of freedom shown in equations (2abcd). If this energy is supplied periodically at high frequencies or in sudden abrupt bursts, it is possible to monitor the ensuing relaxation process. We will concern ourselves only with those methods which influence the vibrational energy levels leading to measurement of vibrational relaxation times.

Shock waves have been successfully used to measure vibrational relaxation at temperatures from one to several thousand degrees Kelvin (26, 69). The effect of a shock wave striking a gas is to

abruptly increase its translational temperature to a thousand degrees or higher leaving the internal degrees of freedom at the preshock temperature. By monitoring the temperature of the gas, or a related property such as density, it is possible to observe the length of time required to re-establish equilibrium between the translational and the remaining degrees of freedom.

In a shock heated gas energy is supplied to the translational energy levels and flows into the vibrational energy levels. It is possible to reverse this technique, introducing energy into the vibrational degrees of freedom and measure the subsequent time lag as the translational and rotational degrees of freedom equilibrate. Relaxation times measured for the forward and reverse processes will be identical for similar temperatures as can be proven using the principle of microscopic reversibility.

In the optic-acoustic effect (14, 97) a gas is illuminated by infrared radiation of modulated intensity. In subsequent collisions the vibrationally excited molecules exchange this energy with the translational degrees of freedom increasing the kinetic temperature of the gas. Since the light source is modulated, the gas will alternately heat and cool producing a sound wave due to the periodic pressure changes in the cell. By increasing the frequency of the modulation it is possible to establish a non-equilibrium condition between the vibrational and thermal energy states of the molecule. At this

time a phase difference will appear between the modulation of the incident radiation and the emitted sound wave. The vibrational relaxation time is determined from the degree of phase lag and the frequency of modulation of the light source.

A technique closely related to the optic-acoustic method is laser excited vibrational fluorescence (40, 73, 109). Here the molecules studied are specially selected and possess a molecular absorption line coincident with a laser wavelength. The laser permits excitation of a large number of molecules into a single vibrational energy state from which fluorescence is observed to occur. By measuring the phase shifts between the fluorescence and the modulated laser beam over a wide range of frequencies and gas pressures it is possible to obtain vibrational relaxation times for specific rate processes.

One promising method, still in the development stage, is that of infrared-microwave double resonance (24, 86). In this technique, a modulated infrared source is used to excite chosen vibrational energy levels. A microwave spectrometer with Stark modulation then monitors subsequent transitions in the rotational energy levels of selected vibrational energy states. Ideally, it should be possible to excite a single vibrational state and then measure the rates of energy transfer to each additional vibrational energy level in the molecule. Such information is necessary if one ever wishes to

separate, one from the other, the many rate constants which combine to give the single relaxation time most commonly observed in energy transfer studies.

Much greater detail regarding the many variations of experimental techniques which may be employed in energy transfer studies can be found in the monographs by Cottrell and McCoubrey (12) and by Stevens (98). Yet to be discussed is one important means of studying vibrational energy transfer in gases. This is the measurement of the velocity and absorption of ultrasound as a function of frequency. Historically this was the first method employed to observe vibrational relaxation (76) and remains today the source of the great majority of available data. High frequency sound waves vary the statistical energy equilibrium at sufficient speeds until the vibrational energy levels can no longer follow the periodic fluctuations in external energy. This is reflected in an anomalous absorption as energy is irreversibly lost and as a velocity dispersion due to the alteration of the effective heat capacity of the gas.

The velocity of sound in an ideal gas is described in equation (5)

$$V_i^2 = \frac{\gamma RT}{M} = \frac{RT}{M}\left(1 + \frac{R}{C_v}\right) \qquad (5)$$

Since the molecular weight and the gas constant, R, are invariant and the temperature of the gas can be measured accurately, it is

possible to make quite accurate measurements of the heat capacity. The heat capacity is a function of the Boltzmann energy distribution summed over the translational, rotational, and vibrational energy levels (electronic levels are rarely accessible to room temperature) and $C_v$ may be written $C_v = C^{tr} + C^{rot} + C^{vib}$. At high sound frequencies the vibrational heat capacity, $C^{vib}$, decreases to zero and the resulting velocity dispersion may be fitted to a relaxation equation. Since the bulk of the dispersion is due to the low lying energy states which contribute heavily to $C^{vib}$, ultrasound measurements do have the disadvantage that little can be learned concerning the higher lying energy levels.

Although a variety of standard methods are available for velocity measurements, the procedure used in this work is a novel optical diffraction technique developed in this laboratory (36, 65, 100). In this method, a column of nearly planar ultrasonic waves generated in the gas acts as a pseudograting and diffracts light rays passing parallel through the sound field. The diffraction phenomenon is a result of the sinusoidal variation of the index of refraction in the gas produced by the compressions and rarefaction accompanying the ultrasound waves.

The diffraction of light by ultrasound, especially in liquids, has been the subject of numerous studies in the past and much of the early work has been summarized by Bergmann ( 4, p. 248-335). In contrast

to the mild success and advance of the method in liquids (5), studies of ultrasound diffraction in gases has been severely limited due to very feeble diffraction intensities. Usage of a laser light source (36) and the introduction of coronagraph optics (100) have overcome the previous intensity problems. Presently the utility of the optical diffraction method as a means to study vibrational energy transfer in gases is comparable to the standard instruments used in high frequency velocity measurements.

# THEORY

## (2.1) Theoretical Correlations to Energy Transfer

The rate at which a system can be changed from one stationary state to another under the influence of a perturbing force is evaluated in quantum mechanics using time-dependent perturbation theory. Here the coefficients of the eigen functions describe the rate of change, and the square of the coefficient of a particular energy state gives the probability of finding the system in that state at a given time. The probability that a molecule originally in stationary state $\psi_n$ will be found in $\psi_m$ is given by

$$P_{nm} = |A_m(t)|^2 \qquad \text{where}$$

$$\frac{d}{dt} A_m(t) = -\frac{2\pi i}{h} \int \Psi^*_m H' \Psi_n \, d\tau \tag{6}$$

and $H'$ is the perturbation causing the transition and $\Psi_m$, $\Psi_n$ are time dependent wave functions.

### Landau-Teller Procedure

The problem to which we wish to apply equation (6) is the deactivation of a vibrational energy level in a diatomic molecule, BC, experiencing a head on collision with an atom A. In addition to assuming a one dimensional interaction we will also consider the

vibrational states of the diatomic molecule to be those of a harmonic oscillator and that the dynamics of the encounter may be treated using classical mechanics.

Since the time dependent wave function is the product of two functions, one involving the time alone and the other the coordinates alone

$$\Psi_n(x,t) = \psi_n(x)\,\varphi_n(t) = \psi_n(x)e^{\frac{-2\pi i}{h}E_n t} \tag{7}$$

equation (6) may be written using just the harmonic oscillator wave functions.

$$\frac{d}{dt}A_m(t) = \frac{-2\pi i}{h}e^{\frac{2\pi i}{h}(E_m - E_n)t}\int \psi_m^* H'\psi_n\,dx \tag{8}$$

Upon simplification, equation (8) reduces to

$$\frac{d}{dt}A_m(t) = -\frac{i}{\hbar}H'_{mn}(t)\exp(2\pi i\nu t) \tag{9}$$

where $(E_m - E_n) = h\nu$ and $H'_{mn}(t)$ is the matrix element of the perturbation.

The interaction, $H'$, responsible for the deactivation of the oscillator, may, as shown below, be approximated as linear in the normal coordinate of the vibration. The form of the perturbation to be considered, then, is $H' = x\,F(t)$, where $F(t)$ describes the repulsive forces experienced by the oscillator and atom undergoing a head on collision. $F(t)$ is initially zero, builds to a maximum at the

distance of closest approach and again falls to zero. The function is also even if we set $t = 0$ at the distance of closest approach and assume that the dynamics of the encounter are unaffected by energy transfer.

The probability that vibrational energy transfer will proceed from the oscillator state $\psi_n$ to $\psi_m$ during a collision is found by inserting the expression for $H'$ into equation (9), integrating, and squaring the result.

$$P_{nm} = |A_m(t)|^2 = \frac{4X_{mn}^2 I^2}{\hbar^2} \tag{10}$$

where

$$X_{mn} = \int_{-\infty}^{+\infty} \psi_m^* \psi_n \, x \, dx \tag{10a}$$

and

$$I = \int_0^{\infty} F(t) \cos(2\pi\nu t) \, dt \tag{10b}$$

The harmonic oscillator functions are given by

$$\psi_n = N_n e^{-\xi^2/2} H_n(\xi), \quad \xi = \sqrt{\alpha}\, x \tag{11}$$

where

$$\alpha = (4\pi^2 M\nu / h)$$

and $N_n$ is a normalizing constant, $H_n(\xi)$ is the Hermite polynomial, and $M$ and $\nu$ are the reduced mass and frequency of the oscillator.

The matrix elements of the coordinates of the harmonic

oscillator, $X_{mn}$, are readily solved and the results have been described in many places, for example Pauling and Wilson (75, p. 80-82). The transition matrix, $X_{mn}$, is zero except for $m = n \pm 1$, when its values are

$$X_{v, v+1} = \sqrt{\frac{v+1}{2a}} \tag{12a}$$

$$X_{v, v-1} = \sqrt{\frac{v}{2a}} \tag{12b}$$

where $v$ is the vibrational quantum number.

Two important properties concerning vibrational energy transfer have been introduced with the solution of the harmonic oscillator matrix elements. The first is that once the transition probability between the ground state and the first excited state is known, the probabilities for all other levels are also known. Since $P_{nm}$ is proportional to $X^2_{mn}$, squaring equations (12a) and (12b) indicates the relationship $P_{01}:P_{12}:P_{23}\ldots = 1:2:3\ldots$ or in general

$$P_{v,\ v-1} = v\, P_{10} \tag{13a}$$

$$P_{v,\ v+1} = (v+1)\, P_{01} \tag{13b}$$

where the relationship between $P_{01}$ and $P_{10}$ is given by the Boltzmann equation.

$$P_{01} = P_{10}\, e^{\frac{-h\nu}{kt}} \tag{13c}$$

The second consequence resulting from the harmonic oscillator approximation is the introduction of the selection rule $\Delta v = \pm 1$. For simple molecules, at least, this rule appears to be obeyed reasonably well. Hooker and Millikan (44) have shown, for example, that vibrational excitation of the second overtone in carbon monoxide proceeds at least nine times out of ten by successive quantum transitions rather than by the direct $v = 0 \rightarrow 2$ process.

For a transition from the first excited level to the ground state, the square of the matrix element is

$$X_{10}^2 = \frac{1}{2a} = \frac{\hbar}{4\pi\nu M} \tag{14}$$

The probability for deactivation of the first excited state is, upon substitution of equation (14) into equation (10)

$$P_{10} = \frac{2I^2}{h\nu M} \tag{15}$$

The calculation of $I$ introduces additional approximations and the stepwise procedure is given in Cottrell and McCoulrey (12, p. 126-128). The value of $F(t)$ is determined using the classical equation of motion to describe the encounter. The interaction forces occurring during the collision are approximated using

$$V(r) = V_o \exp(-r/\ell) \tag{16}$$

where $r$ is the distance between the atoms $A$ and $B$ for an

$A + BC$ collision, and $\ell$ is the repulsion length parameter. The longer ranged potential forces are neglected in this treatment. For the collision of $A$ with a diatomic molecule, $B_2$,

$$r = X - \frac{1}{2}(r_e + x) \tag{17}$$

where $X$ is the translational coordinate and $x$ is the vibrational coordinate. The potential function may then be written

$$V(X, x) = V_o e^{r_e/2\ell} e^{-X/\ell} e^{x/2\ell} \tag{18}$$

which to a first order approximation is for $x \ll 1$

$$V(X, x) \approx V_o e^{r_e/2\ell} e^{-X/\ell}(1 + \frac{1}{2}\frac{x}{\ell}) \tag{19}$$

The $F(t)$ defined above becomes $\frac{V_o}{2\ell} e^{r_e/2\ell} e^{-X/\ell}$ expressed as a function of time by the solution of the classical motion $X = X(t)$. The evaluation of equation (10b) now proceeds by contour integration (12, p. 127) and $I$ is found to be

$$I = 4\pi^2 m\nu\ell \exp(\frac{-2\pi^2\nu\ell}{v}) \tag{20}$$

where

$$m = \frac{m_A(m_B + m_C)}{m_A + m_B + m_C}$$

and $m$ is the reduced mass of the encounter, and $v$ is the relative velocity of the colliding particles at infinite distance before the collision.

Inserting the value for $I$ into equation (15) gives the probability for vibrational deactivation shown earlier in equation (4)

$$P_{10} = A \exp\left(\frac{-4\pi^2 \nu \ell}{v}\right) \tag{21}$$

where

$$A = \frac{32\pi^4 m^2 \nu \ell^2}{hM}$$

and $A$ is a unitless number on the order of 100 - 1000.

The concluding step in evaluating $P_{10}$ is to average equation (21) over all relative velocities in the gas

$$P_{10} = \frac{A}{N} \int_0^\infty \exp\left(\frac{-4\pi^2 \nu \ell}{v}\right) dN \tag{22}$$

where $N$ is the total number of molecules per unit volume and $dN$ is the fraction of molecules with approach velocities in the range $v_o$ and $v_o + dv_o$. The Maxwell distribution law for relative motion is

$$dN = N v_o \left(\frac{m}{kT}\right) \exp\left[\frac{-mv_o^2}{2kT}\right] dv_o \tag{23}$$

For vibrational deactivation the difference between the approach and receding velocities is $h\nu$.

$$mv^2 - mv_o^2 = h\nu \tag{24}$$

Upon substitution of equations (23) and (24) into equation (22), the expression for $P_{10}$ becomes

$$P_{10} = A\left(\frac{m}{kT}\right) \exp\left(\frac{h\nu}{2kT}\right) \int_0^\infty v \exp\left(\frac{-4\pi^2 \nu \ell}{v} - \frac{mv^2}{2kT}\right) dv \qquad (25)$$

The integral shown in equation (25) can not be evaluated in closed form.

By assuming that the behavior of $P_{10}$ is principally dominated by the exponential term, it is possible to evaluate $P_{10}$ by determining the relative velocity for which an inelastic collision is most likely to occur. This occurs when

$$\frac{d}{dv}\left(\frac{4\pi^2 \nu \ell}{v} + \frac{mv^2}{2kT}\right) = \left(-\frac{4\pi^2 \nu \ell}{v^{*2}} + \frac{mv^*}{kT}\right) = 0 \qquad (26)$$

or at a velocity

$$v^* = \left(\frac{4\pi^2 \nu \ell kT}{m}\right)^{1/3} \qquad (27)$$

Substitution of this velocity, $v^*$, for $v$ in the exponential portion of equation (25) indicates

$$P_{10} \text{ varies as } \exp\left[-\frac{3}{2}\left(\frac{16\pi^4 \nu^2 \ell^2 m}{kT}\right)^{1/3}\right] \qquad (28)$$

This relationship lists the important parameters in vibrational-translational energy transfer and predicts what trends one might expect for different oscillator frequencies, a change in temperature, or a variation in the reduced mass of the interaction.

The actual evaluation of the integral in equation (28) is shown in Herzfeld and Litovitz (37, p. 262-266) and involves the neighborhood

of velocities near $v^*$ with the pre-exponential velocity term considered a constant equal to $v^*$. The treatment is valid only if the exponential function falls off steeply on both sides of the velocity maximum. The results, which are an extension of the well known Landau and Teller (56) expression, are shown in equation (29)

$$P_{10} = A \sqrt{\frac{2\pi}{3}} \left(\frac{\epsilon'}{kT}\right)^{1/6} \exp\left[-\frac{3}{2}\left(\frac{\epsilon'}{kT}\right)^{1/3} + \frac{h\nu}{2kT}\right] \qquad (29)$$

with the abbreviation $\epsilon' = m(4\pi^2 \nu \ell)^2$.

Absolute transition probabilities are not calculated using equation (29) due to the rather unrealistic molecular model used in the development. It is significant, however, that the trends indicated in the exponential term have been experimentally verified. Shock tube investigations have shown for many simple gases that log of deactivation probability is indeed linear with the inverse cube root of the temperature (69). While graphs of $P_{10}$ vs $m^{1/3}\nu^{2/3}$ have not yielded linear relationships (74), it is true that as the vibrational frequency of BC decreases and the reduced mass of the encounter decreases, the probability for energy transfer increases. Lambert and Salter (54) have found that plots of $Z_{10}$ (where $Z_{10} = 1/P_{10}$ and is the number of collisions per deactivation) against $\nu_{min}$, the lowest vibrational frequency in the molecule, provide roughly linear results with two broad classes of compounds distinguishable. The first group contains compounds with no hydrogen atoms and the second

group, exhibiting much faster relaxation times, contain two or more hydrogen atoms.

Schwartz, Slawsky and Herzfeld Method

Before comparisons between theoretical and experimental collision probabilities can be performed it is necessary to treat the collision model more realistically. Improvements might be expected if any of the following changes were made. 1) Treat the dynamics of the encounter quantum mechanically; 2) Introduce a more realistic interaction potential; 3) Expand the coordinate system to three dimensions; 4) Consider direct and indirect encounters; 5) Assess the importance of rotational energy level occupation on vibrational energy transfer; 6) Improve upon the basic approximation that transition probabilities are given by first order time dependent perturbation theory [see, for example, Secrest and Johnson (90)].

The problem facing the theoretician can be stated rather succinctly. The very simple collision models, although physically unrealistic, can be solved without introducing a great number of severely limiting assumptions. A more sophisticated model, while describing the interaction more accurately, begins to lose ground as formal simplifications are introduced into the calculations. In such instances the theoretician always faces the temptation to increase the physical significance of his model by introducing a few variable parameters

which are fit to existing experimental data.

The best known theoretical development using a more realistic collision model is the method of Schwartz, Slawsky, and Herzfeld (88, 89). Their model, to a certain extent, does take into account the first three improvements listed above. Although the best results are obtained for homonuclear diatomic molecules, the method also allows one to calculate transition probabilities in polyatomic molecules (103). This has been done for a large number of molecules and in many cases the calculated and experimental values agree within a factor of ten (101, 103). The least accurate results are obtained when treating either polar molecules or molecules with low moments of inertia about one or more axes.

The three dimensional SSH results for an atom A colliding with a molecule BC is shown in equation (30).

$$P_{10} = \left(\frac{r_c}{r_o}\right)^2 \frac{e^{\frac{\epsilon}{kT}}\left(1 - e^{\frac{-h\nu}{kT}}\right)}{Z_o\, Y(2,2)} \frac{m_B^2 + m_C^2}{2(m_B + m_C)^2} P_{10}(LT) \qquad (30)$$

where

$$Y(2,2) = 0.76\left(1 + 1.1\,\frac{\epsilon}{kT}\right)$$

and $Z_o$ is a steric factor arbitrarily set equal to three, $r_c$ is the distance of closest approach, $r_o$ and $\frac{\epsilon}{k}$ are constants in the Lennard-Jones formula, and $P_{10}(LT)$ is the Landau Teller result shown in equation (29).

The remarkable agreement between the quantum mechanical solution and the semiclassical Landau Teller results shown above has been observed by Rapp (82). He has obtained similar results using purely classical mechanics and notes when the semiclassical, and classical methods are developed completely, the results are identical with the SSH solution at the classical limit. Rapp distinguishes between collisions of atom A with either end of the molecule BC which was not done in our development of the Landau Teller expression. Accordingly his results do not show the discrepancy in the ratio of the oscillator masses as ours does upon comparison with Herzfelds results. The significance of different theoretical methods has been stressed in a recent review article by Rapp and Kossal (83) which is quite extensive in its coverage.

## Vibrational-Rotational Energy Transfer

One remaining topic to assess is the importance of rotational energy level occupation on vibrational energy transfer. The Lambert Salter plot mentioned previously suggested two classes of compounds, those possessing two or more hydrogen atoms and those which do not. Since molecules containing hydrogen atoms generally possess low moments of inertia, and therefore, classically speaking, rather large rotational velocities, the increased efficiency of energy transfer may be due to rotational motion.

Millikan and Osburg (71) have firmly established that rotational energy level occupation does affect vibrational relaxation when they demonstrated that para-$H_2$ relaxes vibrationally excited CO molecules more than a factor of two faster than ortho-$H_2$ does.

Cottrell and coworkers have experimentally measured and calculated the relaxation time ratios for the hydrides and deuterides of methane (15), silane (15), phosphine (16), and arsine (11). They have found that the deuterated molecules relax more slowly than the hydrides dispite their rather lower vibrational frequencies. This is in direct contradiction to the predictions based on the SSH method. The theoretical expressions derived by Cottrell for vibrational-rotational energy transfer do predict the correct relaxation ratios for the hydrides and deuterides within ten percent with the exception of arsine which disagrees only by a factor of two.

Moore (74) has derived a simple two parameter model for vibrational-rotational energy transfer applicable to molecules in which the rotational velocities of the atoms are greater than the translational velocity of the molecule. The probability for vibrational deactivation is obtained by substituting the rotational analogues for velocity and reduced mass into equation (21) of the Landau Teller development. The method proceeds by averaging over the thermal distribution of angular velocities in the gas. The resulting equation has been adjusted to fit experimental data using a steric factor $Z_o$ and the repulsive

energy range parameter, $\ell$. One exponential in the probability equation tends to dominate the results and it is remarkable that most data can be fit within a factor of two or three to the simple relationship

$$P_{10} = 7.7 \exp\left(\frac{-1.78\, I\nu^2\ell^2}{d^2T}\right)^{1/3} \qquad (31)$$

where $I$ is the moment of inertia in Amu $\text{Å}^2$, $d$ is the distance from the axis of rotation to the peripheral atom in Å, $\nu$ is the oscillator frequency in $cm^{-1}$, and $\ell$, defined previously, equals 0.12 Å.

The ability to fit a wide range of data to the simple expression shown in equation (31) may or may not be a valid test for vibrational-rotational energy transfer due to the initial adjustment of two parameters. Moore's method has been applied to other systems, however, and with rather satisfying results (8, 95, 96).

Sharma has recently performed quantum mechanical calculations on the $CO_2$-$H_2$ (92) and $CO_2$-$N_2$ (93) systems and finds that the negative temperature dependence exhibited by both gas mixtures (92, 104) can be accounted for by considering long range forces and rotational energy level occupation. There are no adjustable parameters in his theory. The SSH method incorrectly predicts a positive temperature dependence for the $CO_2$-$H_2$ and $CO_2$-$N_2$ systems.

Despite the recent investigations into the subject of vibrational-rotational quantum exchange, the actual importance of such processes

has not been conclusively established. It is difficult to assess for any given molecule whether vibrational deactivation occurs predominately through the translational or the rotational degrees of freedom. Also, although the rotational energy levels are apparently involved in energy transfer, the exact nature of the interaction is not satisfactorily understood.

## (2.2) Propagation of Ultrasound in Gases

The study of the velocity of sound as a function of sound wave frequency provides a convenient probe with which to study vibrational relaxation processes. At frequencies near one MHz the sound wave is varying the statistical equilibrium of the external degrees of freedom with such rapidity that the vibrational degrees of freedom may no longer follow the fluctuations. The general theory of sound propagation in fluids and the accompanying relaxation phenomena is well known. It has been found convenient to derive the relaxation equations for an ideal gas and to apply nonideality corrections to experimental velocity measurements before comparing with the theoretical expressions.

### Relaxation Equations

Except at very high frequencies, sound waves are propagated adiabatically and reversibly. The velocity at which sound is

transmitted is determined by the relationship between the pressure and density of the gas as shown in equation (32).

$$V^2 = (dP/d\rho)_s \tag{32}$$

Using standard thermodynamic relations, equation (32) may be developed in terms of an ideal gas; or, using a more precise equation of state, in terms of a real gas. For an ideal gas, reversible adiabatic pressure changes follow the relationship

$$P = k\rho^{\gamma} \tag{33}$$

where $k$ is a constant and $\gamma$ is the ratio of specific heats.

Substituting equation (33) into (32) and using the ideal equation of state gives the velocity expression disucussed earlier in equation (5)

$$V_i^2 = \frac{RT}{M}\left(1 + \frac{R}{C^{tr} + C^{rot} + C^{vib}}\right) \tag{34}$$

The principle of the equipartition of energy, from classical mechanics, states that each external degree of freedom contributes $1/2\ R$ to the heat capacity of the molecule and each vibrational degree of freedom, $R$. At room temperature the translational and rotational energy levels are classically distributed and the principle of equipartition of energy is applicable. The vibrational contribution to the heat capacity, based on the harmonic oscillator approximation, is

given in equation (35) for a molecule containing (3n-6) vibrational degrees of freedom.

$$C^{vib}/R = \sum_{j=1}^{3n-6} \left(\frac{h\nu_j}{kT}\right)^2 e^{\frac{-h\nu_j}{kT}} \left(e^{\frac{-h\nu_j}{kT}} - 1\right)^{-2} \qquad (35)$$

Rather than evaluate equation (35) directly to obtain $C^{vib}/R$, it is more convenient to use available tables which list the harmonic oscillation contributions to the thermodynamics functions (77, 105).

At higher frequencies the sound waves begin not to equilibrate with the internal degrees of freedom, and the vibrational contribution to the heat capacity decreases to zero. Herzfeld and Rice (38) first accounted for the resulting velocity dispersion through the development of a relaxation equation giving the vibrational relaxation time of the gas. The form of the velocity equation used most often was derived by Kneser (50) and is shown in equation (36).

$$V_i^2 = \frac{RT}{M}\left[1 + R\left(\frac{C_o + C_\infty \omega^2 \tau^2}{C_o^2 + C_\infty^2 + \omega^2 \tau^2}\right)\right] \qquad (36)$$

where $C_o$ and $C_\infty$ represent the static and high frequency heat capacities, respectively, and $\omega$ is the angular frequency of the sound wave.

Equation (36) reduces to the normal velocity expression for very low frequencies (when $\omega\tau << 1$)

$$V_o^2 = \frac{RT}{M}\left(1 + \frac{R}{C_o}\right) \qquad (37)$$

and at high frequencies ($\omega\tau >> 1$) reduces to equation (38).

$$V_\infty^2 = \frac{RT}{M}\left(1 + \frac{R}{C_\infty}\right) \tag{38}$$

Kneser's results may be rearranged in terms of $V_o^2$ and $V_\infty^2$ to give a convenient form of the relaxation equation.

$$\tau^2 = \left(\frac{C_o}{2\pi f C_\infty}\right)^2 \left(\frac{V^2 - V_o^2}{V_\infty^2 - V^2}\right) \tag{39}$$

Using equation (39) it is possible to determine the relaxation time of a gas with just one velocity measurement at a frequency within the dispersive region. The standard practice, however, is to calculate a theoretical dispersion curve of $V_i^2$ versus (f/P) based on equation (39). This is fitted to the experimental data and the relaxation time is determined from the frequency, $f_c$, at the inflection point of the curve.

$$\tau = \frac{1}{2\pi f_c} \frac{C_o}{C_\infty} \tag{40}$$

The relaxation equations just presented are valid for polyatomic molecules in which all of the vibrational specific heat is associated with a single relaxation time. For the few molecules where there is a large frequency discrepancy between modes, the rate of energy transfer through such modes may be slow enough to provide a bottleneck in the series relaxation process. In such instances, two relaxation times might be expected to occur. The theoretical sound velocity

equation for a doubly relaxing gas may be derived from the basic equations for sound dispersion given by Richards (84). This has been done by Valley and Legvold (107) and the results are shown in equation (41).

$$V_i^2 = \frac{RT}{M}\left[1 + R\left(\frac{C_o + A\omega^2 + B\omega^4}{C_o^2 + D\omega^2 + E\omega^4}\right)\right] \tag{41}$$

where

$$A = (C_\infty + C_2)\tau_1^2 + (C_\infty + C_1)\tau_2^2$$

$$B = C_\infty \tau_1^2 \tau_2^2$$

$$D = (C_\infty + C_2)^2 \tau_1^2 + (C_\infty + C_1)^2 \tau_2^2 + 2C_1 C_2 \tau_1 \tau_2$$

$$E = C_\infty^2 \tau_1^2 \tau_2^2$$

and $\tau_1$, $\tau_2$ represent the relaxation time for the first and second steps, respectively, and $C_1$, $C_2$ represent the heat capacity that lags in the first step and in the second step, respectively.

The experimental relaxation parameter $\tau$ represents a bulk relaxation process summed over many oscillator states. Comparisons between such bulk processes and the individual collision probabilities calculated in section (2.1) are possible due to the relationship between the relaxation time and the rate constants for the harmonic oscillator [see, for example, Herzfeld and Litovitz (37, p. 86-90)]. This relationship is shown in equation (43) for a molecule possessing (3n-6) vibrational degrees of freedom.

$$\frac{1}{\tau} = Z P_{10} C_1^{vib} \left( \sum_{j=1}^{3n-6} C_j^{vib} \right) \left(1 - e^{\frac{-h\nu_1}{kT}}\right) \qquad (43)$$

$C_1^{vib}$ and $\nu_1$ denote the heat capacity and frequency of the lowest vibrational mode in the molecule and $Z$ is the number of collisions per molecule per second.

The calculation of the collision frequency is generally based on the kinetic theory expression for a gas of rigid spheres, namely,

$$Z = 4n\sigma^2 \left(\frac{\pi kT}{m}\right)^{1/2} \qquad (44)$$

where $n$ is the number of molecules per unit volume, $\sigma$ is the collision diameter, and $m$ is the molecular mass. Should the Lennard Jones parameters be available, more accurate values of the collision frequency can be calculated using equation (45),

$$Z = 4n\sigma^2 \Omega (2, 2)^* \left(\frac{\pi kT}{m}\right)^{1/2} \qquad (45)$$

where the function $\Omega (2, 2)^*$ has been tabulated in Appendix I-M of Hirshfelder, Curtis, and Bird (39)

Real Gas Behavior

In order to apply the relaxation equations discussed in the preceding section, experimental velocity measurements must be corrected to ideality. Deviations from ideal gas behavior may be described using the virial equation of state

$$\frac{PV}{nRT} = 1 + B_p P + C_p P^2 + \ldots \tag{46}$$

where $B_p$ and $C_p$ are the second and third virial coefficients with respect to pressure. At moderate pressures only the second virial correction need be retained to provide an adequate equation of state. Using equation (46) (with $C_p$ set equal to zero) and the velocity expression shown in equation (32), it is possible to derive the relationship between the real and ideal sound velocities in a gas. This has been done, for example, by Cottrell and McCoubrey (12, p. 8-10) and is reproduced in equation (47)

$$V^2 = V_i^2 \left[ 1 + \left(\frac{2S}{RT}\right) P \right] \tag{47}$$

where

$$S = B_v + \frac{RT}{C_v} B_v' + \frac{(RT)^2}{2C_v C_p} B_v''$$

and $C_v$, $C_p$ are the heat capacities at constant volume and constant pressure, respectively, and $B_v$, $B_v'$, and $B_v''$ represent the second virial coefficient with respect to volume and its first and second temperature derivatives.

Since $B_v = B_p RT$, equation (47) could just as easily have been written in terms of $B_p$. However, the virial equation expanded in terms of $\left(\frac{n}{V}\right)$ has proven to be more useful than equation (46) and most available data is for $B_v$.

The nonideality parameter S, shown in equation (47), may

also be written in terms of the reduced second virial coefficient, $B^*$, as indicated in equation (48)

$$S = b_o [B^* + (\gamma - 1) B_1^* + \frac{(\gamma-1)^2}{2\gamma} B_2^*] \tag{48}$$

where

$$b_o = \frac{2}{3} \pi N \sigma^3$$

and $N$ is Avogudro's number and $B_1^*$, $B_2^*$ represent the first and second temperature derivatives as defined in Hirshfelder, Curtiss, and Bird (39, p. 232).

The most convenient means to evaluate equation (47) is to use experimental virial data which has been fitted to an empirical equation of the form

$$B_v = f + gT^{-1} + hT^{-2} \tag{49}$$

where $f$, $g$, and $h$ are variable parameters.

In many instances virial data have been used to determine intermolecular potential functions and only these force constants are available. The relationship between the second virial coefficient, $B_v$, and the potential function, $V(r)$, for spherical molecules is shown in equation (50)

$$B_v = 2\pi N \int_0^\infty (1 - e^{-V(r)/kT}) r^2 dr \tag{50}$$

where $r$ represents the distance between interacting molecules.

For nonpolar molecules a commonly used intermolecular potential energy function is the Leonard-Jones (6-12) potential.

$$V(r) = 4\epsilon \left[\left(\frac{\sigma}{r}\right)^{12} - \left(\frac{\sigma}{r}\right)^{6}\right] \tag{51}$$

where the parameters $\sigma$ and $\epsilon$ have the dimensions of length and energy. Hirschfelder et al. (39, p. 1114) have tabulated solutions of equation (50) in terms of $B^*$, $B_1^*$, and $B_2^*$ using the Lennard Jones potential. This allows the direct evaluation of $S$ using equation (48).

The expression for the second virial coefficient shown in equation (50) may readily be solved in terms of the square well potential function. Even though this potential model is unrealistic, the presence of three adjustable parameters $R$, $b_o$, and $\epsilon/k$, provide an accurate representation of $B_v$, $B_v'$, and $B_v''$, even for many polar molecules. Should the force constants for the square-well potential be available, they may be substituted into equations (52abc) to obtain virial data.

$$B_v = b_o \left[1 - (R^3 - 1)(e^{\epsilon/kT} - 1)\right] \tag{52a}$$

$$B_v' = b_o (R^3 - 1) \frac{(\epsilon/k)}{T^2} e^{\epsilon/kT} \tag{52b}$$

$$B_v'' = -b_o (R^3 - 1) \frac{(\epsilon/k)}{T^3} \left[2 + \frac{(\epsilon/k)}{T}\right] e^{\epsilon/kT} \tag{52c}$$

The Berthelot equation of state, shown in equation (53), provides a rather good representation of the temperature variation of the second

virial coefficient.

$$(P + \frac{n^2 a}{TV^2})(V - nb) = nRT \qquad (53)$$

where $n$ is the number of moles of gas, and $a$ and $b$ are empirial constants. The Berthelot equation may be multiplied out and rearranged in the form of a virial equation as shown in equation (54) [see, for example, Kauzmann (49, p. 34-40)].

$$\frac{PV}{nRT} = 1 + [b - \frac{a}{RT^2}] \frac{n}{V} + b^2(\frac{n}{v})^2 + \ldots \qquad (54)$$

from which the second virial coefficient, $B_v$, is seen to be

$$B_v = b - \frac{a}{RT^2} \qquad (55)$$

The empirical parameters $a$ and $b$ can be related to the critical constants for the gas by subjecting the Berthelot equation of state to the necessary restraints ($dP/dV = 0$ and $d^2P/dV^2 = 0$) and evaluating the coefficients. The resulting expression, equation (56),

$$B = \frac{9}{128} \frac{RT_c}{P_c} [1 - 6 (\frac{T_c}{T})^2] \qquad (56)$$

may be used in conjunction with equation (47) to obtain accurate values of $S$, but only for nonpolar molecules.

Translational Dispersion

At high ultrasound frequencies, when the wavelength of sound is

approaching the mean free path in the gas, the adiabatic condition governing sound propagation breaks down and equation (32) is no longer valid. The resulting increase in velocity, known as translational (or viscothermal) dispersion, is another type of nonideality correction to be subtracted from experimental velocity measurements. Among the available theories for translational dispersion, the exact Navier-Stokes and Burnett equations are both acceptable up to a few hundred MHz/atm, after which the Burnett equation is the more accurate (28).

The Burnett propagation equation for a monatomic Maxwellian gas is given by Greenspan (29) as

$$k^6\left(-\frac{21}{125}\frac{1}{r^4} - \frac{18}{25}\frac{i}{r^3}\right) + k^4\left(-\frac{97}{50}\frac{1}{r^2} + \frac{9}{10}\frac{i}{r}\right)$$

$$+ k^2\left(1 + \frac{23}{10}\frac{i}{r}\right) + 1 = 0 \qquad (57)$$

where

$$k = \left(\alpha + \frac{i\omega}{V_{tr}}\right)\frac{V_o}{\omega}$$

$$r = \frac{V_o^2 \rho}{\gamma \omega \eta}$$

and $k$ is a normalized propagation constant, $r$ is related to the Reynolds number for the gas by $r = (Re/\gamma)$, $\alpha$ is the amplitude absorption coefficient, $\eta$ is the viscosity and $(V_{tr}/V_o)$ gives the fraction of translational dispersion.

An approximate solution to equation (57) has been given in the

form of a series expansion (29)

$$k = i + \frac{7}{10}\frac{1}{r} - \frac{43}{40}\frac{i}{r^2} - \frac{4203}{2000}\frac{1}{r^3} + \ldots \qquad (58)$$

from which the dispersion relationship is

$$V_o = V_{tr}\left(1 - \frac{43}{40}\frac{1}{r^2} + \ldots\right) \qquad (59)$$

The approximate solution shown in equation (59) is valid for a monatomic gas and gives satisfactory results up to 100-200 MHz/atm (7).

Greenspan (29) has modified the Burnett equation to a diatomic gas and finds only a slight change in the approximate solution.

$$V_o = V_{tr}\left(1 - 0.985\frac{1}{r^2}\right) \qquad (60)$$

Holmes and coworkers (41, 42) have tested the modified Burnett equation using diatomic, as well as polyatomic, molecules over a wide range of frequencies. They find that the Burnett equation for diatomics can be directly used for polyatomic molecules with satisfactory results.

Translational dispersion in gases may, therefore, be approximately evaluated using equation (60) arranged in a slightly more convenient form (57).

$$V_{tr} = V_o\left[1 + B\eta^2(f/P)^2\right] \qquad (61)$$

where $\eta$ is viscosity in cgs units, $(f/P)$ is in MHz/atm, and $B$ is a constant equal to 48 for a monatomic gas and 44 for a polyatomic gas.

In most all instances, translational dispersion below ten MHz/atm is insignificant and use of equation (61) is unnecessary.

## (2.3) Diffraction of Light by Ultrasonic Waves

The suggestion that light could be diffracted by ultrasonic waves was first advanced by Brillouin (10) in 1921 while treating the theoretical aspects of the scattering of light by thermal density fluctuations. The experimental verification of Brillouins prediction was achieved ten years later by Debye and Sears (18) and also by Lucas and Biquard (59). Since then many investigators have studied this phenomenon under a variety of experimental conditions. In most all cases, however, the work pertained to liquids where the effect is far more pronounced. Most of the early theoretical ground work can be accredited to Raman and Nath (78, 79, 80, 81). In addition to giving the correct relationship for the angular separation of the diffracted orders, their papers also provided the first acceptable theoretical description of the intensity distribution over several different orders of diffraction. The theoretical treatment of ultrasonic diffraction has been the subject of numerous investigations and a monograph on the subject has been written by Berry (5). Also, the subject has been

reviewed rather extensively by Bergmann (4, p. 248-335), Born and Wolf (6, p. 593-610), and by Martinez (64, p. 37-54).

Contrasting the progress in liquids, interest in the theoretical aspects of the problem in gases has been slight. The evaluation of the wave equation for diffraction in a gas is necessarily more complex due to the rapid absorption of the ultrasound energy. Absorption does not occur to any appreciable extent in liquids and has been neglected in the theoretical problem. This prevents the direct application of the available intensity formulas to gases, but one can expect that at increasingly higher gas pressures the intensity formulas will be applicable as an approximation.

To illustrate what effect the introduction of an absorption term has on the diffraction intensities, we will compare theoretical results based on a nonabsorbing medium to results where acoustic absorption is allowed to occur.

David (17) has treated the nonabsorbing case and describes the index of refraction varying with the sound wave frequency as

$$n = n_o + n_1 \cos\left(\frac{2\pi z}{\Lambda}\right) \qquad (62)$$

where $n$ is the instantaneous index of refraction, $n_o$ is the index of refraction in the absence of the sound field, $n_1$ is the amplitude change in the index of refraction due to the pressure wave and $z$ is the direction of sound propagation. A convenient form of David's results

may be presented as the ratio of first order diffraction intensities shown in equation (63)

$$\frac{I(+)}{I(-)} = \left[\frac{(\bar{\beta} - \frac{1}{2}) \sin(\bar{\beta} + \frac{1}{2})\, \sigma}{(\bar{\beta} + \frac{1}{2}) \sin(\bar{\beta} - \frac{1}{2})\, \sigma}\right] \tag{63}$$

where

$$\sigma = \frac{\pi \lambda d}{\Lambda^2}$$

$$\bar{\beta} = \frac{\Lambda}{\lambda} \beta$$

with the limiting restraint that

$$\frac{\pi \lambda d}{2\Lambda^2} << 1 \tag{64}$$

for the intensity ratio to be valid.

In equation (63) the subscripts + and - correspond to deflection of the diffracted light with or against the direction of the sound field and $\lambda$ is the wavelength of incident light, $\Lambda$ is the ultrasound wavelength, $\beta$ is the angle between the light rays and sound wave front, and $d$ is the path length through the sound field.

Two cases of equation (63) are of special interest. The first is the expression for zero incidence of the light rays which is

$$\frac{I(+)}{I(-)} = 1 \qquad \text{when} \quad \beta = 0 \tag{65}$$

The second point of interest is when the intensity ratio is at a

maximum. This occurs at the Bragg condition when $\beta = \pm \lambda/2\Lambda$.

$$\frac{I(+)}{I(-)} = \left(\frac{\sigma}{\sin \sigma}\right)^2 \qquad \text{when} \quad \beta = \frac{-\lambda}{2\Lambda} \tag{66}$$

These results can be compared with those obtained by Decius (19) who included acoustic absorption and described the index of refraction varying with the sound wave frequency as

$$n = 1 + n_1 e^{-\alpha z} \cos\left(\frac{2\pi z}{\Lambda}\right) \tag{67}$$

which represents the conditions in a dilute gas. Decius has taken the special case for zero incidence and has solved the wave equation for the light diffraction according to the perturbation method developed by Brillouin (10). His results indicate that at zero incidence the ratio of first order diffraction intensities is given by

$$\frac{I(+)}{I(-)} = e^{-4K\sigma} \qquad \text{when} \quad \beta = 0 \tag{68}$$

where

$$K = \frac{\alpha\Lambda}{2\pi}$$

Equation (68) predicts that in regions of rapid acoustic absorption the diffraction intensities will be asymmetrical even at zero incidence in contrast to the case in liquids. Since soundwaves are irreversibly absorbed during vibrational relaxation, Decius' results indicate that intensity asymmetry for the first order diffraction

images should occur in this region. In addition, his theoretical development for an absorbing gas indicates image broadening of the Lorentz shape will also take place.

The intensity ratio predicted using equation (68) for gases undergoing vibrational relaxation depends on the specific heat being lost and may be as large as a factor of three or four. This effect tends to be lost due to the diffraction asymmetry which occurs if the zero incidence condition is not accurately met. A calculation of the intensity ratio at the Bragg angle indicates this factor can be dominant. The importance of critical alignment of the light rays with the sound field is shown upon evaluation of the Bragg angle which is only a few milliradians for most gases.

The subject of intensity asymmetry of the first order diffraction images is discussed in further detail in the Appendix.

Fortunately, the relationship upon which velocity calculations are based is independent of the angle of incidence and is shown in equation (69)

$$n\lambda = \Lambda \sin n\theta = \frac{V}{f} \sin n\theta \tag{69}$$

where $n$ is the diffraction order and $\theta$ is the angle of diffraction. Diffraction angles are very small which allows $\sin \theta$ to be written as

$$\sin\theta = \frac{\delta}{(\delta^2 + F^2)^{\frac{1}{2}}} \approx \frac{\delta}{F} \tag{70}$$

where $\delta$ is the diffraction distance between the zero order and first order diffraction light and $F$ is the distance at which the diffraction image was recorded, or the focal length of the lens system. The error introduced by the approximation shown in equation (70) is less than 0.01 percent with the optical diffraction apparatus used in these studies. Introducing the $\sin\theta$ approximation into the diffraction equation gives the resulting velocity expression shown in equation (71)

$$V = \frac{\lambda f F}{\delta} \tag{71}$$

Systematic errors in velocity measurement may be minimized by using a standard gas of known velocity to determine the focal length of the optical system. This reduces equation (71) to the final form used in evaluating experimental velocity data.

$$V_{exp} = V_{std} \left( \frac{2\delta_{std}}{2\delta_{exp}} \right) \left( \frac{f_{exp}}{f_{std}} \right) \tag{72}$$

where $2\delta$ represents the distance between the $(+1)$ and $(-1)$ diffraction images.

# EXPERIMENTAL

## (3.1) Description of Optical Diffraction Apparatus

The optical diffraction instrumentation used in this investigation has been described previously by Martinez (64, p. 55-81) and also by Strauch (99, p. 23-43). To avoid repetition only recent modifications of the apparatus will be discussed at any length.

In the optical method, ultrasonic waves generated in the gas act as a pseudo-grating and diffract light rays passing parallel through the cell. A diagram of the apparatus is shown in Figure 1. The light source is a Spectra-Physics model 131 He-Ne gas laser rated at one mW output power at 6328 Å. The laser beam is expanded and collimated by passage through a 150 mm telescope objective, a pinhole aperture and the first cell lens. Both cell lens (constructed from borosilicate crown glass) are plano-convex f/20 lenses of 1500 mm focal length. As the light field passes parallel through the sound field generated by the quartz transducer, a small (usually $< 0.01\%$) percentage of the intensity will be diffracted. The diffraction images, as well as the zero order laser beam, are focused on the first lens of the coronagraph optics.

The coronagraph optics are a simple system of masks and lens originally designed by Lyot (61) for the purpose of studying the solar cornona. The optical problem presented here is similar as it is necessary to photograph weakly diffracted images lying only a few

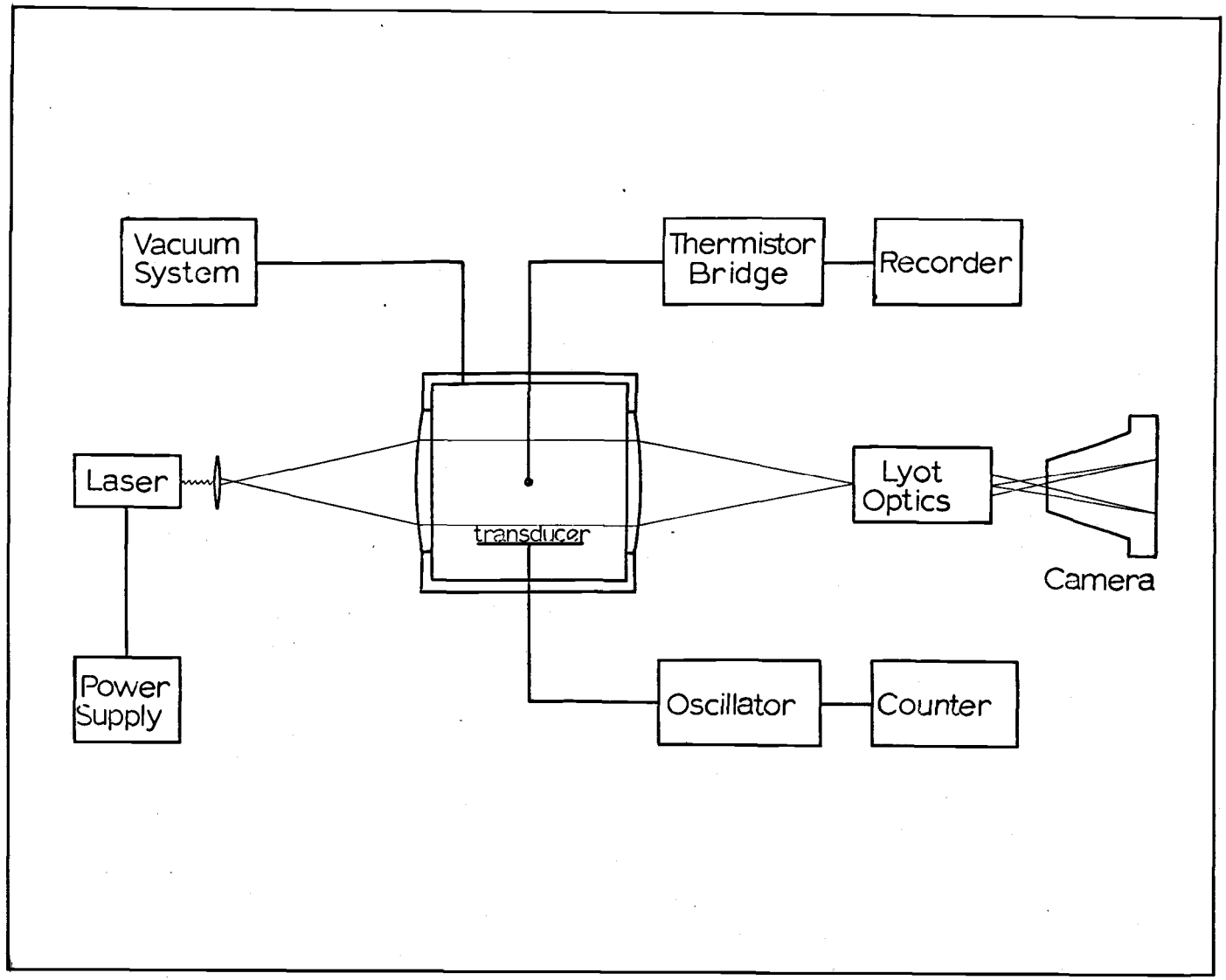


Figure 1. Diagram of optical diffraction apparatus.

millimeters from the very intense undiffracted laser beam. Lyot optics are quite effective in reducing stray background light due to internal lens reflections and to aperture diffraction (which occurs along the edge of the cell lens). A detailed discussion of the design of the coronagraph optical system used here can be found in Strauch (99, p. 23-33) and also in Strauch and Decius (100).

The diffraction images emerging from the Lyot optics are recorded on low sensitivity Kodak type 649-F glass plates. The resolution of this emulsion is extremely high, being approximately 2000 lines/mm. Exposure times are generally between 0.0025-10 seconds, except for very low gas pressures.

The distance between the first order diffraction images usually varies between four to ten millimeters and can be measured to an accuracy of ±0.002 mm using a Gaertner model M1170-342 comparator. The width of the diffraction dots changes from an average of 0.03 mm in nondispersive regions to 0.15 mm in regions of strong acoustic absorption. Under the most severe conditions the images are still capable of being measured to an accuracty of ±0.01 mm.

Photographs are taken using an Orbit Monorail Precision Camera manufactured by Burke and James, Inc. The camera has been bench mounted and rests on a dove-tail slide which allows over 50 exposures to be made on a single 4" x 5" photographic plate. A Synchro Compur Shutter has exposure speeds of 1/400 to 1 second

as well as time.

The Hartley oscillator used to excite the quartz transducer was constructed by Martinez (64, p. 63). Stability of the oscillator is generally one part per million during exposure times. The frequency is monitored using a Hewlett Packard Model 5232A counter. R. F. voltages applied to the transducer usually vary in the 10-150 volt range.

The x-cut quartz transducers used to generate the sound wave in the cell were obtained from Valpey Corporation and have tolerances for flatness and parallelism within ±0.00005". The Brashear method (102) has been used to silver the faces of the crystals. Crystals, 1.75" in diameter, with fundamental frequencies of 0.56, 0.99, 1.07, and 1.78 MHz were used in this study.

Temperature measurements are obtained using an aged, Fenwall GB 32J2 bead thermistor. The bridge circuit is manufactured by E. H. Sargent and Company. The sensitivity of the bridge has been adjusted to one millivolt per degree Centigrade and voltage changes are recorded on a ten mv Brown Class 15 Electronik recording potentiometer. The thermistor was calibrated using a NBS standardized thermometer which is marked off in 0.02°C divisions. The data points have been fitted to a second order curve using a least squares computer program. All calibration data points were found to fall within ±0.05°C of the least squares curve.

The vacuum system for the introduction and removal of gases from the cell is of conventional design and is composed of two parts. An all glass section for use at pressures below one atmosphere consists of a standard taper outlet for the introduction of gas samples, a mercury manometer, a thermocouple vacuum gauge (RCA Model-1946) and a series of two cold traps (one for the collection and disposal of gas samples and the other to protect the vacuum pump). The high pressure section is constructed from 1/4" stainless steel tubing and numerous Whitey valves and contains a system of three stainless steel traps which may be used for the purification and storage of gas samples. Three Swagelok Outlets are available for the direct attachment of gas cylinders to the line. Absolute pressures are measured on a helicoid gauge which reads from 0-200 lbs/in$^2$. The cell itself is constructed from a solid block of aluminum and is capable of withstanding a pressure of ten atmospheres. A detailed cross section diagram of the optical diffraction cell is shown in Figure 2. The individual sections are bolted together and are held pressure tight using O rings.

## (3.2) Operation of the Optical Diffraction Equipment

The basic operation of the optical diffraction apparatus is not difficult and will be described briefly in the following paragraphs. The attainment of high precision velocity data does require a basic

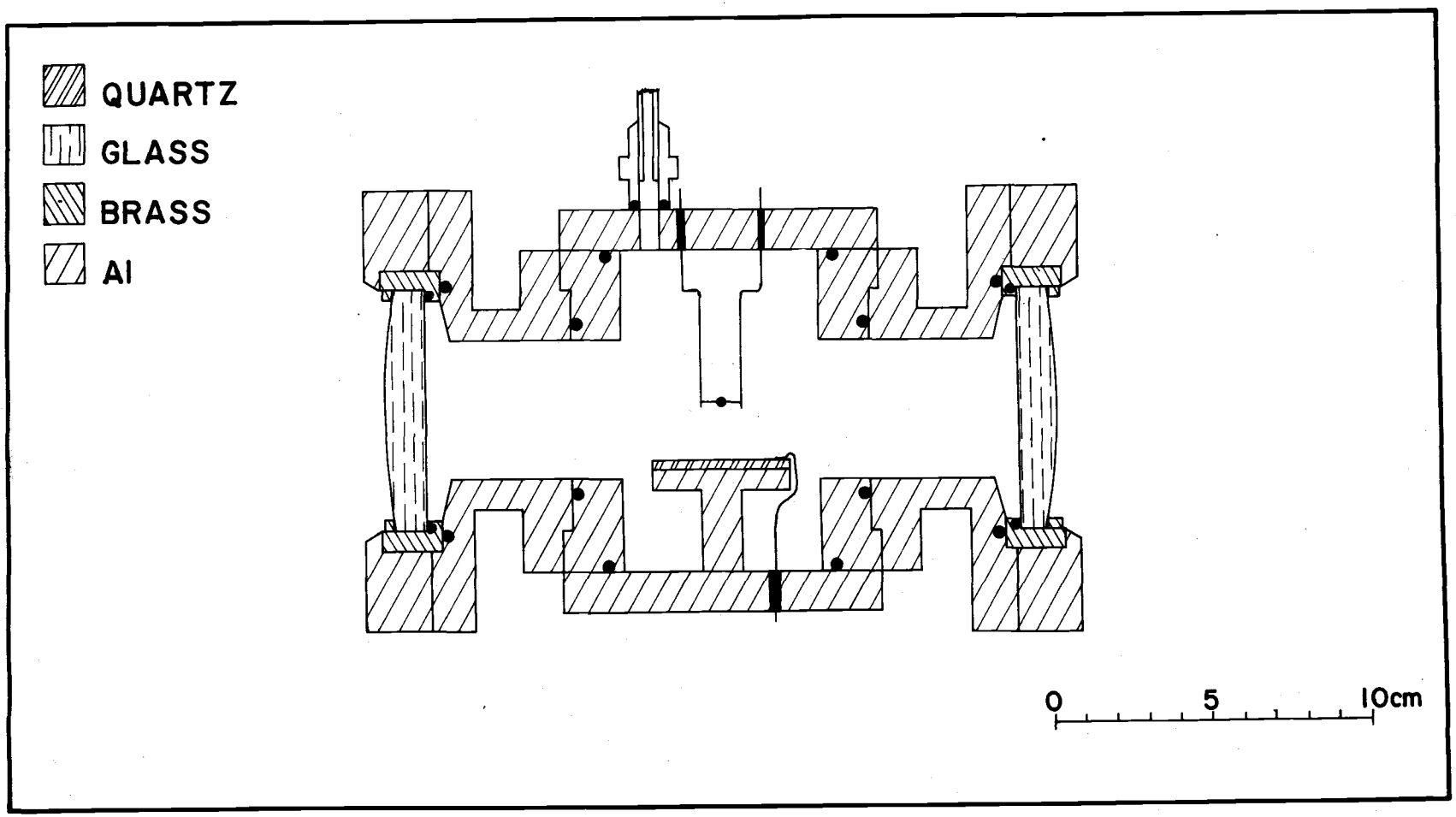


Figure 2. Cross section diagram of the optical diffraction cell.

knowledge of the instrument and the location of possible sources of error. Accordingly, those areas which may influence the overall quality of the results will be presented in somewhat greater detail.

After allowing the Hartley oscillator a sufficient warm-up period (usually one hour) the gas to be studied is introduced into the cell and the oscillator is tuned to obtain a visual diffraction image. Rather than tune to a maximum diffraction intensity it is best to locate a position which gives satisfactory intensity and exhibits a stable resonance without drifting. This allows the use of the same resonant frequency throughout the experiment which is fairly important.

Systematic errors in velocity determinations are minimized by using a standard gas of known velocity to calibrate each diffraction image obtained with the experimental gas. In the past, double exposures were made at a single camera setting, giving a superposition of the diffraction images for the experimental and standard gases. This was done since the diffraction image was established by a slit when the Mercury lamp light source was used. Accurate measurement of the distance between the slit images proved difficult and the superposition of exposures provided a method whereby alignment errors would tend to cancel in the resulting velocity calculations. With the introduction of the laser light source, this practice is no longer followed. The laser yields point images and absolute

distance measurements between diffraction dots are accordingly more reliable. It is still necessary, of course, to match laboratory conditions between the experimental and standard gases as closely as possible.

The Kodak 649-F emulsion used in this work is of extremely high contrast. It is therefore necessary to take several exposures at any given gas pressure to insure a diffraction image suitable for measurement. The method of data taking used in this investigation was first to introduce the standard gas and take a sequence of calibration photographs covering the gas pressures to be studied using the experimental gas. The system would then be evacuated for about an hour, and after flushing the cell several times, the experimental gas photographs were taken. This method yields about six data points per plate and is a fairly rapid procedure as only one gas change occurs during the entire sequence. The proper exposure times for the experimental and standard gases should be determined in advance by photographing a few selected points at varying pressures. Plots of log P versus log t may then be used to estimate exposure times at any selected pressure.

Before commencing a series of experiments, the alignment of the optical system was checked. To insure parallel passage of the light rays through the cell, the pinhole aperture should be accurately placed at the focal length of the first cell lens. The proper

positioning of the pinhole is aided by placing a mirror in the cell and reflecting the image back to the mask. Proper alignment is obtained by adjusting the reflected image to as small a size as possible. When the alignment is complete, the distance from the pinhole to the first cell lens should be the same as the distance from the second cell lens to the point of focus on the Lyot optics. This should be true since the collimating and focusing lenses (which also serve as windows for the ultrasonic cell) have equal focal lengths.

Determining the focal plane of the camera may be done visually by moving the plate holder back and forth or photographically (which is the preferred method).

Adjustment of the cell tilt is rather critical as this determines the intensity ratio for the plus and minus first order diffraction images. Asymmetry effects are exaggerated using a high contrast emulsion and unless the zero incidence requirement is accurately met, distance measurements become less precise. The cell tilt is varied by means of a vertical vernier which also serves as a support for one end of the optical diffraction cell. The distance between the two cell supports is about 100 mm and changing the vernier by 0.1 mm affects an angle change of approximately one milliradian. After visually determining the best cell tilt, photographs should be taken at 0.1 mm distances on both sides of this position. The alignment is most sensitive for gases which give large diffraction angles.

The purity of gas samples may deteriorate while in the optical diffraction cell if the system is not sufficiently air tight. The apparatus should be leak tested before each experiment using the thermocouple vacuum gauge. If the gauge is properly calibrated it is possible to estimate the amount of leakage into the system during an experiment. If the amount of impurity introduced into the cell is sufficient to alter the composition of the gas, the vacuum line should be inspected for possible leakage. Often the problem is associated with outgassing of the system. The high pressure stainless steel tubing used throughout most of the vacuum line is of 1/8" internal diameter and the pumping rate is extremely slow. During active periods of research, the system should always be kept under vacuum between experiments.

Temperature measurement is not completely reliable as the thermistor seems to respond to the R. F. radiation transmitted from the oscillator. This effect can be observed by evacuating the cell and noting the erratic behavior of the bridge circuit when the oscillator is tuned in and out of resonance. Fortunately, the use of a standard gas tends to minimize this problem. For best results, the same resonant frequency should be used with both the standard and experimental gases. The effect diminishes as the oscillator voltage is decreased and, accordingly, the most accurate velocity measurements are made at lower voltages.

Measurement of diffraction in regions of strong acoustic absorption is made easier by a slight modification of the Lyot optics. In the second focal plane of the Lyot optics an inverted image of the illuminated cell appears, but more importantly, (as will be seen shortly) the ultrasonic diffraction grating is visible due to the Schlieren effect. Schlieren photographs of the ultrasound grating in n-pentane and $CCl_2F_2$ are shown in Figure 3. Also included are background photographs of the cell image taken when the transducer was not oscillating. At 2 MHz/atm appreciable soundwave absorption does not occur in n-pentane and the ultrasonic wave train penetrates well into the illuminated area of the cell. The Schlieren photograph of $CCl_2F_2$ was taken in the middle of the gases' vibrational dispersion region. The absorption is so great in this case that the ultrasonic waves are completely absorbed within a few millimeters of the crystal face. With the coronagraph masking system, background radiation is reduced in the second focal plane by employing an iris to remove the circular image of the cell opening. Also an ink dot is placed on the second objective lens to remove the centrally located reflection image. By increasing the size of the mask in this plane to exclude the cell image where diffraction is not occurring, the background radiation can be substantially reduced.

Since diffraction in cases of strong acoustic absorption occurs only within a small portion of the total illuminated area, it is

Background n-Pentane (2MHz/atm)

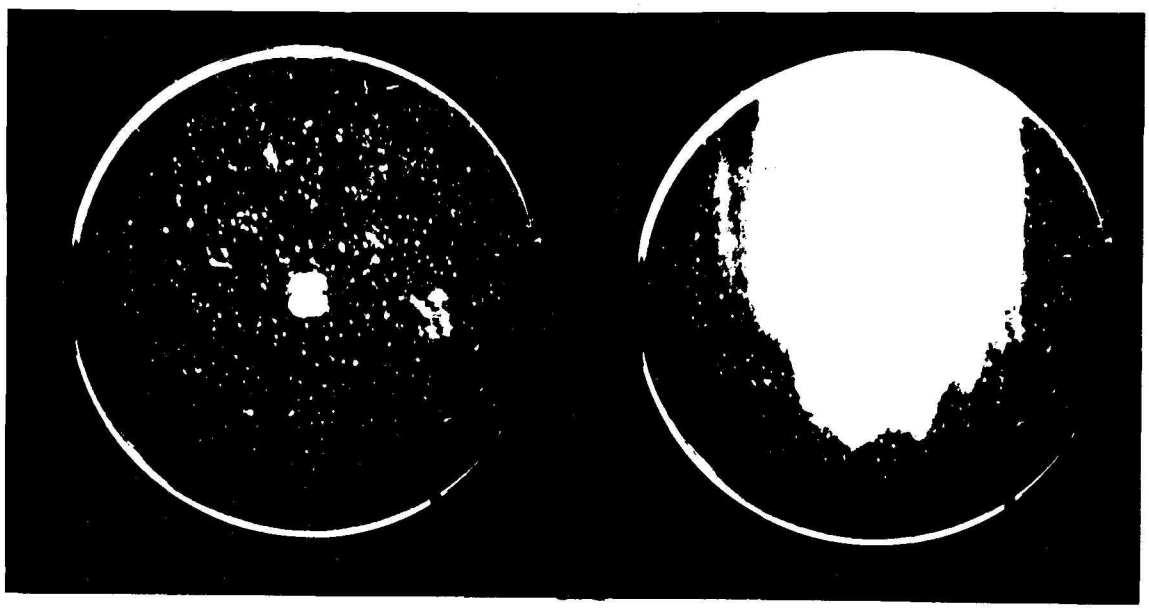

Background $CCl_2F_2$ (1MHz/atm)

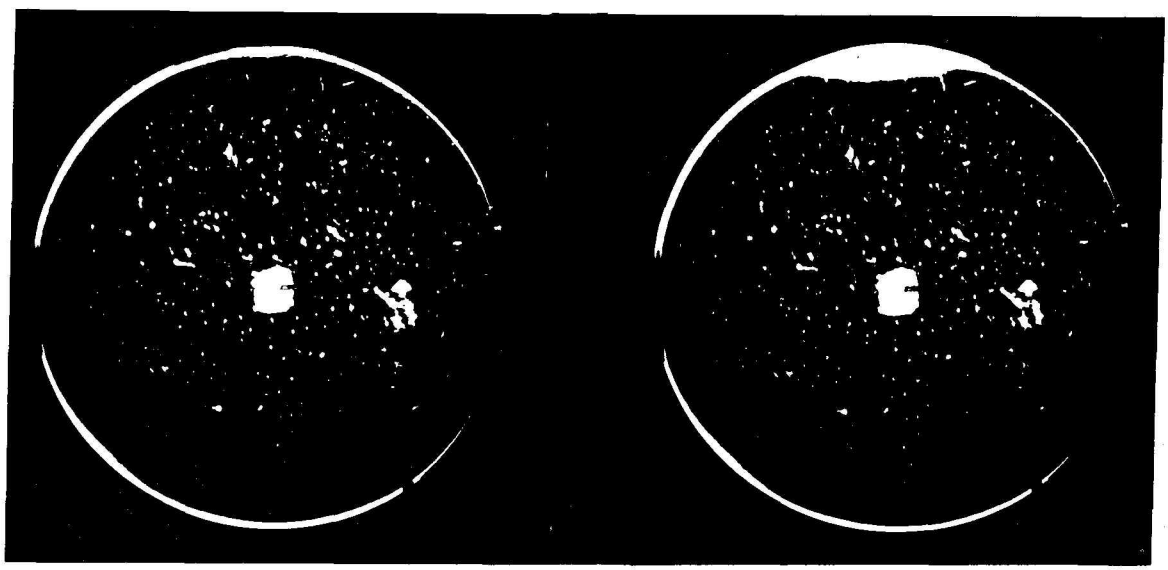

Figure 3. Schlieren photographs of the ultrasound grating in n-pentane and $C Cl_2 F_2$.

beneficial to reduce the diameter of the light beam passing through the cell. Circular apertures ranging in size from 8-26 mm have been made which may be placed in front of the first cell lens. The transducer is then raised until the crystal is almost, but not quite, within the illuminated area. In special instances it may prove feasible to replace the first cell lens with an optical flat and to use the laser beam directly. Attention must be given, however, to the wavelength of sound, as the ultimate resolution of the diffracted image is proportional to the number of illuminated lines in the diffraction grating.

Exposure times at high (f/P) typically run 100 seconds or more. Since image quality is reduced in these regions it would be desirable to switch to a more sensitive emulsion. Usage of Kodak Type V-F photographic plates would reduce exposure times by a factor of 100. The resolving power is better than 225 lines/mm which is more than adequate.

One further consideration when working in difficult regions is to keep the cell lens meticulously clean and free from dust. The procedure for lens cleaning and polishing has been given by Strauch (99, p. 25).

## (3.3) Preparation of Standard and Experimental Gases

### Standard Gases

Standard gases of known velocity are used in the determination of experimental velocities as has been indicated in equation (72). Ideally it is best to select a standard gas whose velocity is close to the gas undergoing investigation. Argon and nitrogen were used throughout the present study and were obtained from Matheson Company. Matheson lists the purity as 99.995% for argon and 99.997% for nitrogen.

The velocity of sound for these gases has been calculated using equation (47). A convenient form of the velocity equation for room temperature calculations is shown in equations (73) and (74) for nitrogen and argon, respectively.

$$\text{(Nitrogen)} \qquad V^2 = (415.515)(1+6.46\times10^{-4}P)\ T(m^2/sec^2) \qquad (73)$$

$$\text{(Argon)} \qquad V^2 = (346.881)(1+5.13\times10^{-4}P)\ T(m^2/sec^2) \qquad (74)$$

where T is in $^{o}K$, P is in atm, and the nonideality corrections have been calculated using the Lennard Jones parameters.

### Ammonia

Anhydrous ammonia was obtained from the Matheson Company

and has a list purity of 99.99% $NH_3$; 0.01% $N_2$. As was noted by Strauch (99, p. 57) and also in this study, gas samples taken from a full cylinder of ammonia contained one to two percent nitrogen. Since ammonia is almost entirely present in the cylinder in liquid form, initial samples might be expected to be rich in nitrogen due to the wide separation of vapor pressures between these two gases.

A convenient means of purification consisted of expanding the gas into the system and condensing liquid ammonia in a stainless steel trap at -78°C. The vacuum line was then evacuated and approximately one half of the sample removed by vacuum fractionation. The remaining half was stored in the trap until needed. Several samples were prepared in this manner and, as indicated in section (4.1), no inconsistencies in the velocity data were obtained.

Allene

A lecture gas bottle of allene was purchased from the Matheson Company. A typical lot analysis provided with the gas listed the impurities as 0.25% oxygen, 0.80% nitrogen, 0.48% carbon dioxide, 0.56% propylene, and 0.68% methyl acetylene. The purification of allene proceeded as follows. The allene was transferred to a stainless steel trap and held under vacuum at -110°C using an ethanol liquid-solid slush. The oxygen and nitrogen appeared to separate from the sample almost immediately but the evacuation procedure

was continued for one hour. Carbon dioxide was removed by vacuum distilling the allene sample several times through a trap containing Linde 4Å molecular sieves. No attempt was made to separate the propylene and methyl acetylene from the allene sample.

Carbon Suboxide

Carbon suboxide samples were prepared by the dehydration of malonic acid with phosphorus pentoxide (57). The by-products of the reaction are water, acetic acid, and carbon dioxide, leaving only a 10% by weight yield of carbon suboxide theoretically attainable. The reagents were mixed in a one liter flask in the following proportions: 20 gm malonic acid, 40 gm ignited sand, and 200 gm phosphorus pentoxide. The preparation entailed a vacuum distillation carried out over a two hour period at a reaction temperature between 140-150°C. The distilled gases were passed through a lime tower and collected in U-tubes for immediate purification. The method of purification followed was similar to that given by Miller and Fateley (67). Carbon dioxide was removed by vacuum evaporation with the raw product held at -110°C for 8-12 hours. The prepurified product was held at -30°C using an o-xylene slush and the carbon suboxide removed by vacuum fractionization.

The final product contained about one ml of carbon suboxide and it proved necessary to repeat the above reaction approximately ten

times to obtain enough sample to perform satisfactory velocity measurements. Carbon suboxide was stored at liquid nitrogen temperatues at all times, except while in the optical diffraction cell. The final product has been analysed on an Atlas CH 4 Mass Spectrometer and a Beckmann IR-7 Infrared Spectrophotometer. The results indicate 3 ± 1% carbon dioxide as the only impurity detectable.

# RESULTS

## (4.1) Ammonia

The velocity of sound in gaseous ammonia has been measured over the range 1.1-13.7 MHz/atm. This investigation is an extension of previous work in this laboratory by Strauch (99, 100) who covered the range 0.15-2.1 MHz/atm. The present velocity measurements failed to detect sound dispersion in ammonia. As an upper limit, our velocity data suggest $\tau < 2$ ns. Jones, Lambert, Saksena, and Stretton (47) have recently found that the rotational and vibrational modes relax together at $\tau = 0.73$ ns. Thus the relaxation of the vibrational degrees of freedom in ammonia is among the fastest reported for a simple molecule. The aspect of the ammonia problem which makes it truly unique is the wide separation of relaxation times between the hydride and deuteride forms. The relaxation time for $ND_3$ is $\tau = 13$ ns (16) which is 18 times slower than for $NH_3$. This behavior is found in no other molecule and cannot be explained in terms of the conventional theories outlined in section (2.1).

### Experimental Data

Real sound velocities in ammonia have been calculated from experimental data using equation (72) and were corrected to 300°K

using the relationship

$$V_{300}^2 = V^2\left(\frac{300}{T}\right) \tag{75}$$

where T is the experimental temperature in $^{o}$K. The experimental sound velocities are listed in Tables 1 and 2 along with the diffraction distances, frequencies, temperatures, and pressures used in the velocity calculations. Nitrogen has been used as a standard gas and the sound velocities shown in Table 1 were calculated from equation (73). Three separate crystals of frequencies 0.996, 1.07, and 1.78 MHz were used in the present measurements. The R. F. voltage applied to the crystals did not exceed 130v. Exposure times varied from 0.0025-70 seconds for gas pressures ranging from 1.0-0.08 atmospheres.

Since the ammonia measurements are in a nondispersive region, the nonideality parameter, S, (identified in equation (47)) has been evaluated experimentally using the velocity data from photographic plate (4-11-68#1). The nonideality correction is linear with pressure as is indicated in Figure 4 and S has been determined from the slope by least squares analysis. The result is S = -150.8±5 cc/mole. This value has been used to calculate the idealized sound velocities shown in Table 2. Using Figure 4, $V_i^2$ can also be evaluated from the intercept. The least squares analysis yields $V_i^2$ = $(19.090\pm0.005)\times10^4 m^2/sec^2$ for the seven data points indicated.

Table 1. Velocity of sound in nitrogen (standard gas).

| Plate Identification | Pressure (atm) | Temperature ($^{o}$K) | Frequency (KHz) | Diffraction Distance (mm) | $V_i^2$ ($\times 10^4$ m$^2$/sec$^2$) | $V_{real}^2$ ($\times 10^4$ m$^2$/sec$^2$) |
|---|---|---|---|---|---|---|
| 8-9-67 #1 | 0.554 | 299.87 | 995.829 | 5.3314 | 12.4601 | 12.4646 |
| " | 0.168 | 300.31 | .683 | 5.3256 | 12.4783 | 12.4797 |
| 4-11-68 #1 | 0.993 | 296.84 | 1069.422 | 6.3133 | 12.3341 | 12.3420 |
| " | 0.724 | 296.75 | .417 | 6.3125 | 12.3304 | 12.3362 |
| " | 0.517 | 296.68 | .413 | 6.3145 | 12.3275 | 12.3317 |
| " | 0.420 | 296.60 | .412 | 6.3137 | 12.3242 | 12.3275 |
| " | 0.318 | 296.53 | .410 | 6.3152 | 12.3213 | 12.3238 |
| " | 0.237 | 296.53 | .408 | 6.3149 | 12.3213 | 12.3231 |
| " | 0.179 | 296.59 | .407 | 6.3147 | 12.3238 | 12.3253 |
| 6-28-68 #1 | 0.982 | 298.67 | 1775.957 | 10.4495 | 12.4102 | 12.4180 |
| " | 0.789 | 298.74 | .952 | 10.4488 | 12.4131 | 12.4194 |
| " | 0.458 | 298.83 | .943 | 10.4484 | 12.4168 | 12.4195 |
| 7-31-68 #3 | 0.157 | 298.60 | 1063.901 | 6.2715 | 12.4073 | 12.4085 |
| " | 0.105 | 299.12 | .881 | 6.2731 | 12.4289 | 12.4298 |
| " | 0.081 | 299.03 | .880 | 6.2702 | 12.4251 | 12.4257 |

Table 2. Ideal velocity of sound in ammonia at 300°K.

| Identification | Pressure (atm) | Temperature (°K) | Frequency (KHz) | Diffraction Distance (mm) | $V^2$ 300°K ($\times 10^4$ $m^2$ $sec^2$) | $V_i^2$ ($\times 10^4$ $m^2$ $sec^2$) | f/P (MHz/atm) |
|---|---|---|---|---|---|---|---|
| 8-9-67 #1 | 0.167 | 301.74 | 995.679 | 4.2994 | 19.0414 | 19.0815[a] | 5.96 |
| " | 0.554 | 301.07 | .986 | 4.3162 | 18.9559 | 19.0891[b] | 1.80 |
| 4-11-68 #1 | 0.992 | 297.10 | 1069.426 | 5.1320 | 18.8599 | 19.0988 | 1.08 |
| " | 0.724 | 297.08 | .421 | 5.1226 | 18.9167 | 19.0908 | 1.48 |
| " | 0.517 | 297.02 | .417 | 5.1168 | 18.9687 | 19.0930 | 2.07 |
| " | 0.418 | 297.03 | .415 | 5.1136 | 18.9807 | 19.0816 | 2.56 |
| " | 0.320 | 297.01 | .412 | 5.1099 | 19.0130 | 19.0894 | 3.34 |
| " | 0.234 | 296.94 | .412 | 5.1064 | 19.0402 | 19.0971 | 4.57 |
| " | 0.180 | 296.94 | .411 | 5.1052 | 19.0515 | 19.0945 | 5.94 |
| 6-28-68 #1 | 0.980 | 298.50 | 1775.957 | 8.5038 | 18.8447 | 19.0801[c] | 1.81 |
| " | 0.792 | 298.54 | .952 | 8.4928 | 18.8906 | 19.0808[d] | 2.24 |
| " | 0.456 | 298.61 | .947 | 8.4736 | 18.9705 | 19.0802 | 3.89 |
| 7-31-68 #3 | 0.157 | 297.91 | 1063.922 | 5.0810 | 19.0373 | 19.0749 | 6.79 |
| " | 0.105 | 298.84 | .892 | 5.0758 | 19.0744 | 19.0998 | 10.10 |
| " | 0.078 | 299.46 | .882 | 5.0674 | 19.0587 | 19.0774 | 13.71 |

Velocities listed on plates 8-9-67 #1 and 6-28-68 #1 are representative of a total of 17 $V^2$ measurements made under similar conditions. The average values are as follows: a) 19.0823; b) 19.0888; c) 19.0796 and d) 19.0841.

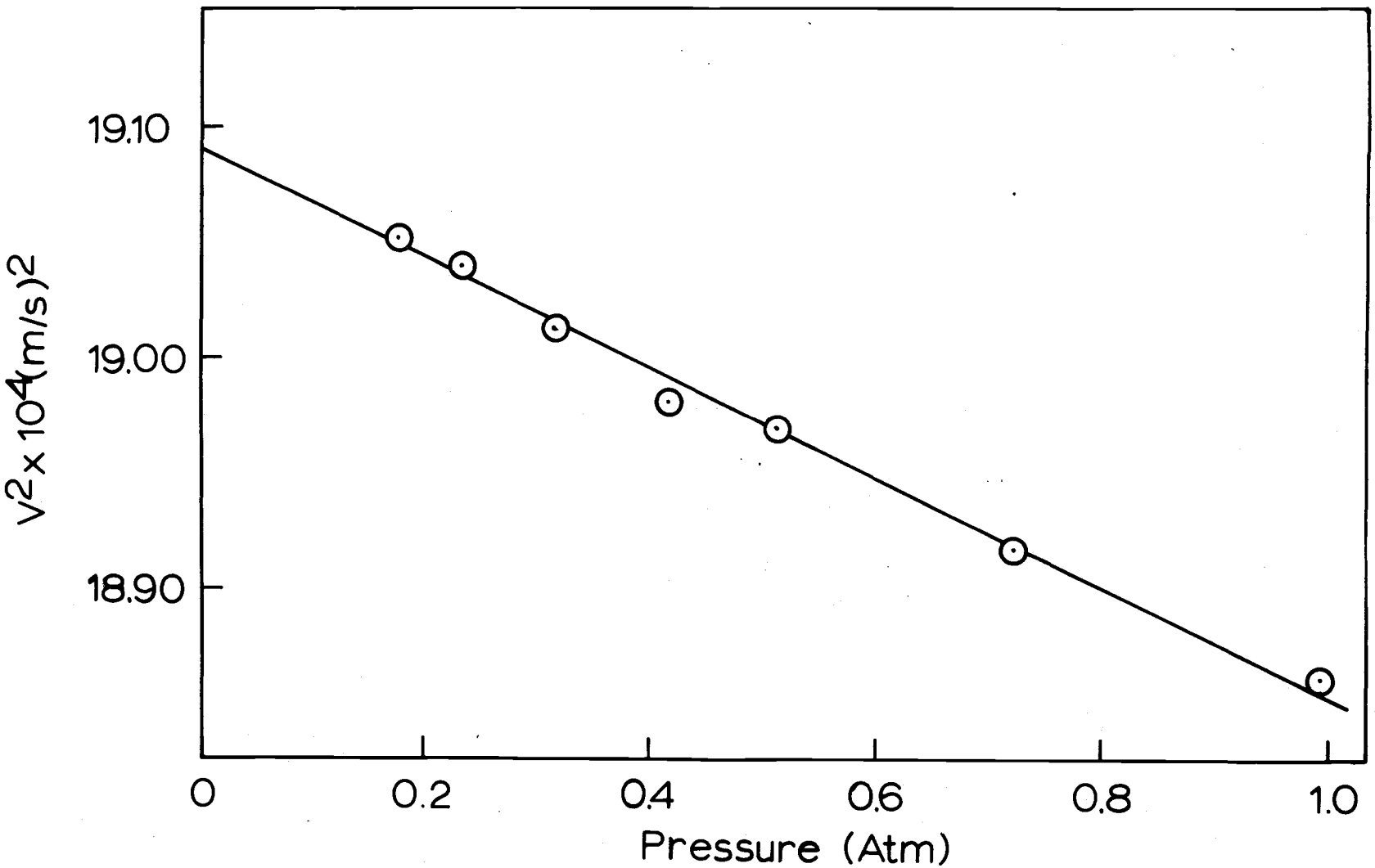


Figure 4. Sound velocity in $NH_3$ at 300°K vs pressure.

Only data from photographic plate (4-11-68#1) has been used to determine the nonideality correction as the parameter S does vary with temperature. Ammonia measurements from this plate all lie within a narrow temperature range, 296.6 ± 0.2° K.

The nonideality correction S = -151 cc/mole at 297°K is in complete agreement with the value obtained by Cottrell, Mac Farlane, and Read (13) (S = -142 ±10 cc/mole at 303°K) and with the virial data of Lambert and Strong(55). A rather fortuitous agreement for ours and Cottrell's value is obtained when S is evaluated using the square well potential for ammonia listed in Hirschfelder, Curtiss, and Bird (39, p. 160). The parameters are: $b_o$ = 30.83 cc/mole, $\varepsilon/k$ = 692°K, and R = 1.268. Using equations (47) and (52abc) we find S = -150.6 cc/mole at 297°K and S = -141.9 cc/mole at 303°K.

The above results disagree somewhat with a recent experimental value obtained by Jones et al. (47) which is S = -195 ± 13 cc/mole at 298°K. Since all measurements are performed at or below one atmosphere, the disagreement listed above does not affect seriously the final idealized velocity values obtained.

## Experimental Results

Idealized sound velocity measurements in ammonia, corrected to 300°K, are shown in Figure 5 along with data also obtained in this laboratory by Strauch and Decius (100). Addition of a small He-Ne

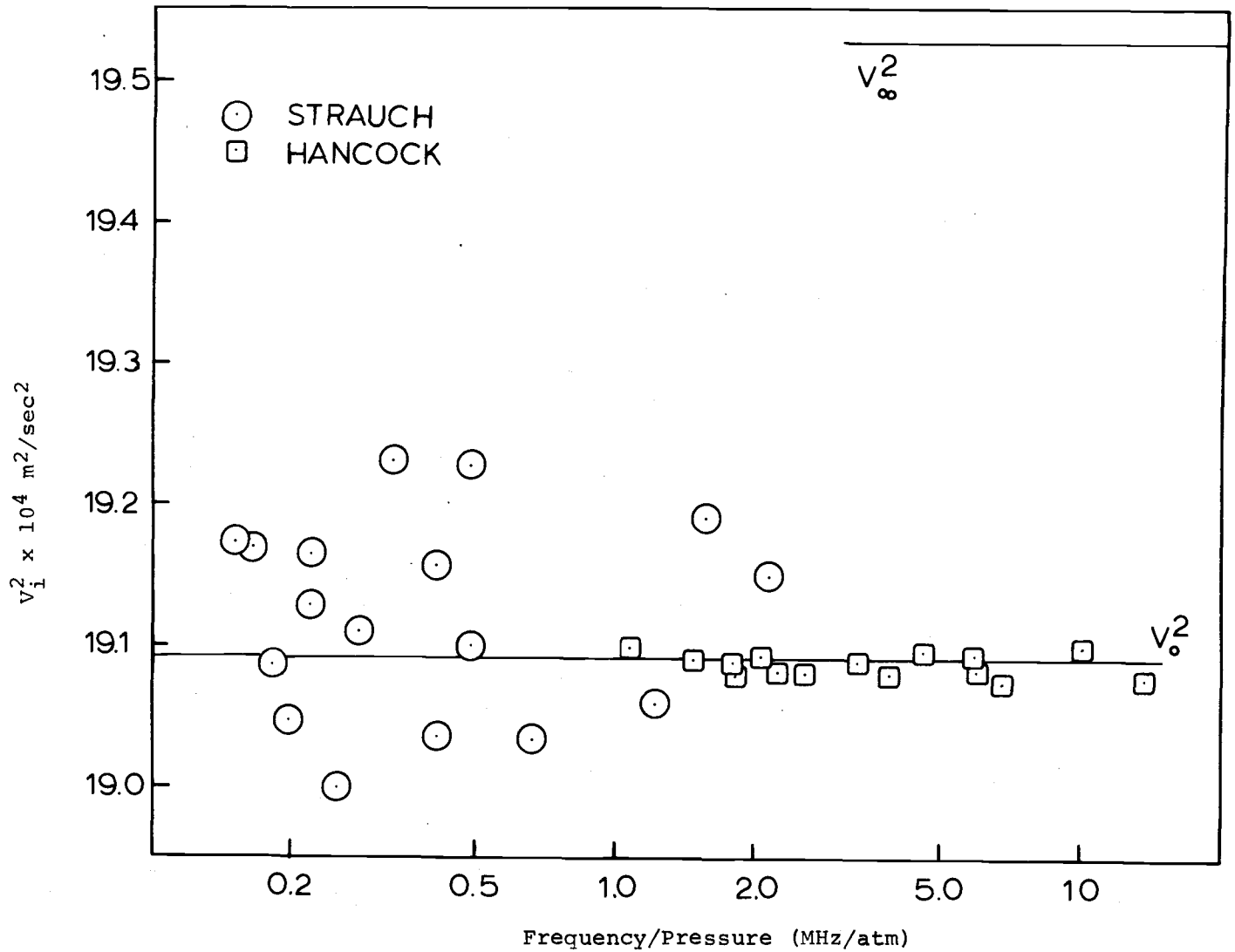


Figure 5. Ideal sound velocity in $NH_3$ at 300°K.

laser, along with some modifications in the experimental procedure, has increased the precision of the velocity measurements from the ±0.18% reported in 1966 to the present ±0.04%.

The ideal velocity of sound in ammonia can be evaluated using equation (34) provided the vibrational specific heat is known with sufficient accuracy. Haar (31) lists the vibrational heat capacity of ammonia as $(C_v/R) = 3.2939 \pm 0.003$. His results are based on spectroscopic data and the methods of statistical mechanics. The partition functions used in his calculations include contributions from vibrational anharmonicity, vibrational-rotational coupling, rotational stretching, and rotational quantum effects. Particular attention was given to the treatment of the rotational and vibrational anharmonic effects due to the $\nu_2$ mode associated with the inversion of the pyramid. The sound velocity based on these calculations is listed below, together with experimental velocities (corrected to 300°K) obtained by Jones et al. (47) and in the present investigation.

$V_i^2 = (19.092 \pm 0.003) \times 10^4 \text{ m}^2/\text{sec}^2$ ($C_v$ from Haar)

$V_i^2 = (19.087 \pm 0.008) \times 10^4 \text{ m}^2/\text{sec}^2$ (this work)

$V_i^2 = (19.084 \pm 0.006) \times 10^4 \text{ m}^2/\text{sec}^2$ (Jones et al.)

The most promising feature of the optical diffraction method is its accuracy, which approaches that which may be attained using spectroscopic data and the methods of statistical mechanics.

The present velocity measurements show no dispersion up to 14 MHz/atm. An upper limit can be placed on the vibrational relaxation time in ammonia by using equation (39). If we assume that a velocity dispersion equal to three times the standard deviation of the data would be detectable, then the vibrational relaxation must be above $\tau < 2$ ns. This observation is in agreement with the results of Jones et al. (47), who find both the vibrational and rotational degrees of freedom relax together at $\tau = 0.73$ ns.

Discussion

The most striking feature in comparing transition rates for ammonia and heavy ammonia is that $NH_3$-$NH_3$ collisions are ten times more efficient in promoting vibrational energy transfer than $ND_3$-$ND_3$ collisions. This efficiency is not found for the hydrides and deuterides of related compounds as may be seen in Table 3. The discrepancy in the collision probabilities between $NH_3$ and $ND_3$ cannot be justified using the conventional theories outlined in section (2.1). This opinion is at least superficially substantiated by the predictions shown in Table 3 for vibrational-translational and vibrational-rotational energy transfer. While rotational effects have been used by some investigators to explain why the hydrides tend to relax faster than the deuterides, this argument does not appear to extend to the ammonia results.

Table 3. Ratios of collision probabilities, $P_{10}(H)/P_{10}(D)$, for the hydrides and deuterides of simple molecules.

| Molecules | Vib-Rot Equation (31) | Vib-Trans SSH Method | $P_{10}(H)/P_{10}(D)$ Experimental | Temperature $^{o}K$ |
|---|---|---|---|---|
| $CH_4$, $CD_4$ | 1.8 | 0.42 (35) | 1.4 (39) | 298 |
| $SiH_4$, $SiD_4$ | 1.4 | 0.2 (41) | 1.4 (39) | 298 |
| $NH_3$, $ND_3$ | 1.3 | ~ 0.8 (78) | 10.0 (78) | 298 |
| $PH_3$, $PD_3$ | 1.1 | 0.1 (41) | 1.5 (40) | 303 |
| $AsH_3$, $AsD_3$ | 1.1 | 0.04 (41) | 0.6 (41) | 303 |
| $H_2O$, $D_2O$ | 1.0 | ~ 1 (84) | 0.8 (83) | 410 |
| HCl, DCl | 1.0 | 0.02 (42) | 2.6 (82) | 700 |
| HBr, DBr | 1.0 | -- | 1.9 (82) | 700 |
| HI, DI | 1.0 | -- | 2.5 (82) | 700 |

Cottrell and Matheson (11) have interpreted the $NH_3$, $ND_3$ problem in terms of the inversion phenomenon. The $\nu_2$ mode in $NH_3$ and $ND_3$ is the vibration associated with the inversion of the pyramid. Each vibrational state in this mode is split into two components and the potential energy function is represented by a double minimum. The spacing for each level is demonstrably more anharmonic in the case of $NH_3$ (20) where the splitting for the first three energy levels of the $\nu_2$ state is 0.66 $cm^{-1}$ ($\nu$=0), 35.7 $cm^{-1}$ ($\nu$=1) and 312.5 $cm^{-1}$ ($\nu$=2). The splitting in $ND_3$(20) is much smaller, for example, 2.4 $cm^{-1}$ for the first excited level of the $\nu_2$ state.

The average time required to penetrate the potential hill is inversely proportional to the energy difference of the two sublevels. If the molecules are viewed classically we can predict the length of time the ammonia molecule will remain in one configuration before suddenly inverting to its mirror image. For the $\nu_2$ ($\nu$=1) levels we find $2.1 \times 10^{14}$ inversions/second for $NH_3$ and $1.4 \times 10^{13}$ inversions/second for $ND_3$. Cottrell and Matheson have compared these inversion times with the period of duration of a molecular collision and have suggested that the probability of an inversion occurring during a collision is quite high for $NH_3$.

If oriented collisions occur in $NH_3$, a sudden inversion would be expected to be highly repulsive if the molecules are sufficiently close. This increase in the sharpness of the force-time relationship

of the encounter means a much shorter repulsive range parameter. As shown in equation (21), a more rapid conversion of kinetic to potential energy increases the probability for an inelastic collision.

Unfortunately, the weakness of the present arguement is rather serious as it is not valid to consider the inversion phenomenon from a classical point of view. Nevertheless, the possibility that the inversion phenomenon may be the most important factor contributing to the highly efficient $NH_3$-$NH_3$ collisions has been brought forth. It is suggested that a more rigorous quantum mechanical calculation along these lines should be pursued. It is also evident that vibration-rotation coupling is important here inasmuch as $NH_3$ is the first example of a molecule in which the heat capacities due to both types of motion disappear together.

(4.2) Allene

The vibrational relaxation time in allene (propadiene) has been determined by sound velocity measurements over the range 0.3-33 MHz/atm. The lower 1/4 of the dispersion region has been observed and the results indicate that all of the vibrational degrees of freedom relax together at $\tau = 5.2$ ns at $300^{\circ}K$. The two lowest vibrational modes in allene ($\nu_{11} = 354\ cm^{-1}$ and $\nu_{10} = 842\ cm^{-1}$) are widely separated and for a small number of gases the presence of such a gap leads to two vibrational relaxation times. This has not been

observed in the present investigation.

Information regarding the physical properties of allene has been summarized by Gallant (25) and the chemistry of allene has been extensively reviewed by Griesbaum (30).

Experimental Data

The velocity of sound in allene at 300°K with argon and nitrogen as standard gases has been determined from laboratory measurements using equations (72), (73), (74) and (75). The sound velocities so obtained are listed in Tables 4 and 5, together with the experimental data necessary for the calculations. Diffraction images were recorded on Kodak 649-F glass plates with the exception of the series (5-9-69#2) where Kodak III-F emulsion was used. Exposure times varied from 0.0025-200 seconds for gas pressures in the range 3.7-0.032 atmospheres. A 1.07 MHz crystal and R.F. voltages ranging from 10-170 volts were used in the generation of the sound wave.

For sound velocities at nine MHz/atm and higher the experimental and standard gas pressures were not matched as accurately as possible. Instead, standard gas pressures were chosen which tended to approximate the diffraction intensity exhibited by the experimental gas. This was necessary in order to extend the range of the instrument as the diffraction intensities recorded for standard gases are very weak at low pressures. Since the purpose of the standard

Table 4. Velocity of sound in argon and nitrogen (standard gases).

| Plate Identification | Pressure (atm) | Temperature ($^{o}$K) | Frequency (KHz) | Diffraction Distance (mm) | $V_i^2$ ($\times 10^4$ $m^2/sec^2$) | $V_{real}^2$ ($\times 10^4$ $m^2/sec^2$) |
|---|---|---|---|---|---|---|
| 5-5-69 #2 (Argon) | 3.74 | 298.08 | 1068.231 | 6.8511 | 10.3398 | 10.3597 |
| " | 2.58 | 298.14 | .230 | 6.8535 | 10.3419 | 10.3556 |
| " | 1.84 | 298.22 | .200 | 6.8535 | 10.3447 | 10.3544 |
| " | 1.29 | 298.26 | .201 | 6.8549 | 10.3461 | 10.3529 |
| " | 0.88 | 298.56 | .200 | 6.8536 | 10.3565 | 10.3611 |
| 5-7-69 #1 (Argon) | 0.630 | 300.94 | 1067.968 | 6.8194 | 10.4390 | 10.4424 |
| " | 0.408 | 301.06 | .963 | 6.8200 | 10.4432 | 10.4454 |
| " | 0.287 | 301.07 | .960 | 6.8221 | 10.4435 | 10.4451 |
| " | 0.209 | 301.17 | .901 | 6.8144 | 10.4470 | 10.4482 |
| " | 0.155 | 301.14 | .904 | 6.8124 | 10.4460 | 10.4468 |
| " | 0.133 | 301.10 | .901 | 6.8124 | 10.4446 | 10.4453 |
| 5-9-69 #1 (Nitrogen) | 0.132 | 297.23 | 1073.666 | 6.3092 | 12.3503 | 12.3512 |
| " | 0.132 | 297.43 | .661 | 6.3054 | 12.3587 | 12.3596 |
| " | 0.132 | 297.54 | .660 | 6.3048 | 12.3632 | 12.3641 |
| " | 0.132 | 297.99 | .641 | 6.2962 | 12.3819 | 12.3828 |
| " | 0.132 | 298.05 | .640 | 6.2948 | 12.3844 | 12.3853 |
| 5-9-69 #2 (Nitrogen) | 0.118 | 298.64 | 1069.551 | 6.2568 | 12.4089 | 12.4097 |
| " | 0.118 | 298.64 | .550 | 6.2733 | 12.4089 | 12.4097 |
| " | 0.118 | 298.64 | .551 | 6.2655 | 12.4089 | 12.4097 |
| " | 0.118 | 298.69 | .550 | 6.2656 | 12.4110 | 12.4118 |
| " | 0.118 | 298.69 | .550 | 6.2605 | 12.4110 | 12.4118 |
| " | 0.092 | 298.82 | .544 | 6.2685 | 12.4164 | 12.4170 |
| " | 0.092 | 298.82 | .554 | 6.2596 | 12.4164 | 12.4170 |
| " | 0.092 | 298.82 | .543 | 6.2546 | 12.4164 | 12.4170 |

Table 5. Ideal velocity of sound in allene at 300°K.

| Plate Identification | Pressure (atm) | Temperature (°K) | Frequency (KHz) | Diffraction Distance (mm) | $V^2_{300°K}$ ($\times 10^4$ $m^2/sec^2$) | $V^2_i$ ($\times 10^4$ $m^2/sec^2$) | f/P (MHz/atm) |
|---|---|---|---|---|---|---|---|
| 5-5-69 #2 | 3.74 | 298.03 | 1068.242 | 8.6098 | 6.6030 | 7.2568 | 0.286 |
| " | 2.58 | 298.06 | .218 | 8.4830 | 6.8032 | 7.2537 | 0.414 |
| " | 1.84 | 298.10 | .202 | 8.4002 | 6.9363 | 7.2578 | 0.580 |
| " | 1.29 | 298.13 | .201 | 8.3444 | 7.0305 | 7.2554 | 0.828 |
| " | 0.88 | 298.29 | .210 | 8.3004 | 7.1044 | 7.2583 | 1.214 |
| 5-7-69 #1 | 0.629 | 301.00 | 1067.976 | 8.2366 | 7.1342 | 7.2431 | 1.698 |
| " | 0.407 | 300.98 | .966 | 8.2124 | 7.1802 | 7.2507 | 2.626 |
| " | 0.286 | 301.14 | .963 | 8.2085 | 7.1979 | 7.2474 | 3.740 |
| " | 0.209 | 301.20 | .902 | 8.1848 | 7.2135 | 7.2497 | 5.105 |
| " | 0.150 | 301.33 | .903 | 8.1740 | 7.2242 | 7.2501 | 7.119 |
| " | 0.105 | 301.38 | .901 | 8.1596 | 7.2475 | 7.2657 | 10.14 |
| 5-9-69 #1 | 0.118 | 298.26 | 1073.659 | 8.2572 | 7.2530 | 7.2738 | 9.07 |
| " | 0.086 | 298.39 | .670 | 8.2458 | 7.2661 | 7.2812 | 12.46 |
| " | 0.0710 | 298.61 | .664 | 8.2325 | 7.2854 | 7.2978 | 15.12 |
| " | 0.0526 | 299.18 | .634 | 8.1906 | 7.3372 | 7.3465 | 20.41 |
| " | 0.0447 | 299.10 | .625 | 8.1740 | 7.3672 | 7.3751 | 24.02 |
| 5-9-69 #2 | 0.0974 | 298.74 | 1069.548 | 8.2133 | 7.2509 | 7.2678 | 10.98 |
| " | 0.0789 | 298.77 | .545 | 8.1839 | 7.3024 | 7.3163 | 13.55 |
| " | 0.0789 | 298.77 | .545 | 8.1948 | 7.2841 | 7.2980 | 13.55 |
| " | 0.0632 | 298.78 | .544 | 8.1739 | 7.3227 | 7.3338 | 16.92 |
| " | 0.0632 | 298.79 | .544 | 8.1746 | 7.3092 | 7.3203 | 16.9 |
| " | 0.0391 | 298.97 | .538 | 8.1128 | 7.4223 | 7.4292 | 27.4 |
| " | 0.0391 | 298.96 | .538 | 8.1160 | 7.4119 | 7.4188 | 27.4 |
| " | 0.0322 | 299.01 | .537 | 8.0826 | 7.4769 | 7.4827 | 33.2 |

gas is to evaluate the focal length of the optical system the selection of the gas pressure should, theoretically, have no effect on the accuracy of the experimental velocity data. On the contrary, the seating of the cell lens may be affected by changes in pressure within the cell. This could be expected to have some effect on the focal length and accordingly, gas pressures should be matched whenever possible. At low pressures, however, the cell lens are held firmly in place by the external pressure and small variations in the internal pressure should not affect the velocity data.

The nonideality parameter used to correct the measured sound velocities in allene is S = -292 ± 1 cc/mole at 298°K. This value was determined experimentally by plotting velocity squared versus pressure outside the dispersion region as shown in Figure 6. The slope was evaluated by least squares analysis and the data is taken from plate (5-5-69#2). Although experimental sound velocities are corrected to 300°K, the nonideality correction strictly applies to the mean temperature over which the velocity measurements were performed. Since the nonideality correction is small to begin with, this second order correction has been neglected.

An estimate of the accuracy of the experimentally determined nonideality parameter, S, has been obtained using the Lennard Jones parameters (34) ($\varepsilon/k$ = 194.9°K and $\sigma$ = 6.43Å) and equation (48). The result finds S = -276 cc/mole at 300°K in fair agreement with the

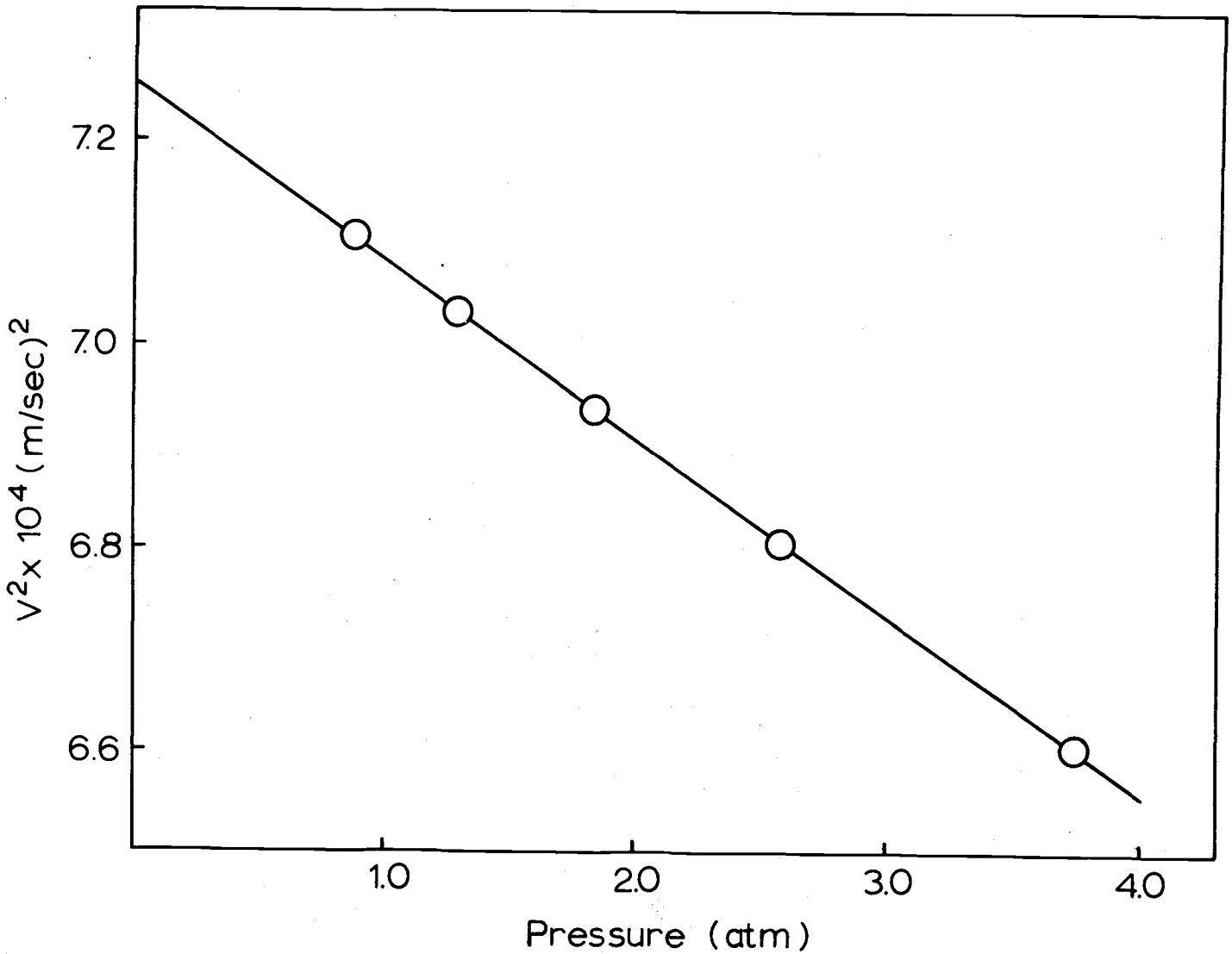


Figure 6. Sound velocity in allene at 300°K vs pressure.

experimental value.

In addition, S has been evaluated using equation (47) with virial data obtained from the Berthelot equation, reported in equation (56). The critical constants for allene are $T_c = 393^oK$ and $P_c = 51.6$ atm (25) and the ensuing calculations yields S = -279 cc/mole at $300^oK$.

Experimental Results

The 11 normal modes of vibration in allene and their contribution to the heat capacity are listed in Table 6. The vibrational heat capacities were calculated using the harmonic oscillator rigid rotor approximation and the spectroscopic data of Lord and Venkateswarlu (58) with the exception of $\nu_9$ which was taken from Mills, Smith and Duncan (72). The large separation between the two lowest frequencies in allene suggests the possibility of double dispersion with the lowest mode relaxing independently of the rest. The total heat capacity would therefore be 6.1123R under static conditions, 4.5820R with the loss of all modes except $\nu_{11}$, and 3.0000 R with the loss of all of the vibrational degrees of freedom. Ideal sound velocities in allene calculated using equation (34) to determine the three limiting velocities yields:

$V_o^2 = 7.2444 \times 10^4 m^2/sec^2$ static velocity

$v_m^2 = 7.5846 \times 10^4 m^2/sec^2$ all modes except $\nu_{11}$ relaxing

Table 6. The vibrational heat capacity of allene at 300°K.

| Vibration | Frequency $cm^{-1}$ | $C_v/R$ |
|---|---|---|
| $\nu_{11}(E)$ | 354 | 1.5820 |
| $\nu_{10}(E)$ | 842 | 0.5962 |
| $\nu_4(B_1)$ | 865 | 0.2805 |
| $\nu_9(E)$ | 999 | 0.3880 |
| $\nu_3(A_1)$ | 1076 | 0.1546 |
| $\nu_7(B_2)$ | 1398 | 0.0552 |
| $\nu_2(A_1)$ | 1440 | 0.0480 |
| $\nu_6(B_2)$ | 1957 | 0.0074 |
| $\nu_1(A_1)$ | 2996 | .0001 |
| $\nu_5(B_2)$ | 3005 | .0001 |
| $\nu_8(E)$ | 3085 | .0002 |

Vibrational total $C_v/R = 3.1123$

$V_\infty^2 = 8.3011 \times 10^4 m^2/sec$ high frequency velocity

Measured sound velocities in allene, corrected for nonideality are shown in Figure 7. The results favor the interpretation that all the vibrational modes in allene relax together with $\tau = 5.2$ ns. The data have been fitted to the theoretical curve for a single relaxation shown in equation (36). The center of the dispersion is located at $f_c = 62$ MHz/atm.

Since it is not immediately apparent from Figure 7 whether the allene data should be interpreted as singly or doubly relaxing, this point will be discussed in greater detail. We have observed a 3.3% velocity dispersion which, as seen from the limiting velocities above, is enough to cover 70% of the dispersion curve for the first step in the multiple relaxation process. The curvature of the dispersion observed in our velocity measurements is much too steep to be associated with a two step relaxation.

In contrast to rate processes which have comparable relaxation times, the term multiple relaxation is generally associated with a separation of steps by a factor of ten or greater. Should the allene data be force fitted to a double dispersion curve we find for the slower process a relaxation time $\tau_1 = 7.0$ ns. Using the present definition of multiple dispersion implies that the deactivation of the lowest mode ($\nu_{11} = 354$ cm$^{-1}$) is equal to or faster than $\tau_2 < 0.7$ ns. While it will not be denied that such a relaxation time is feasible, allene

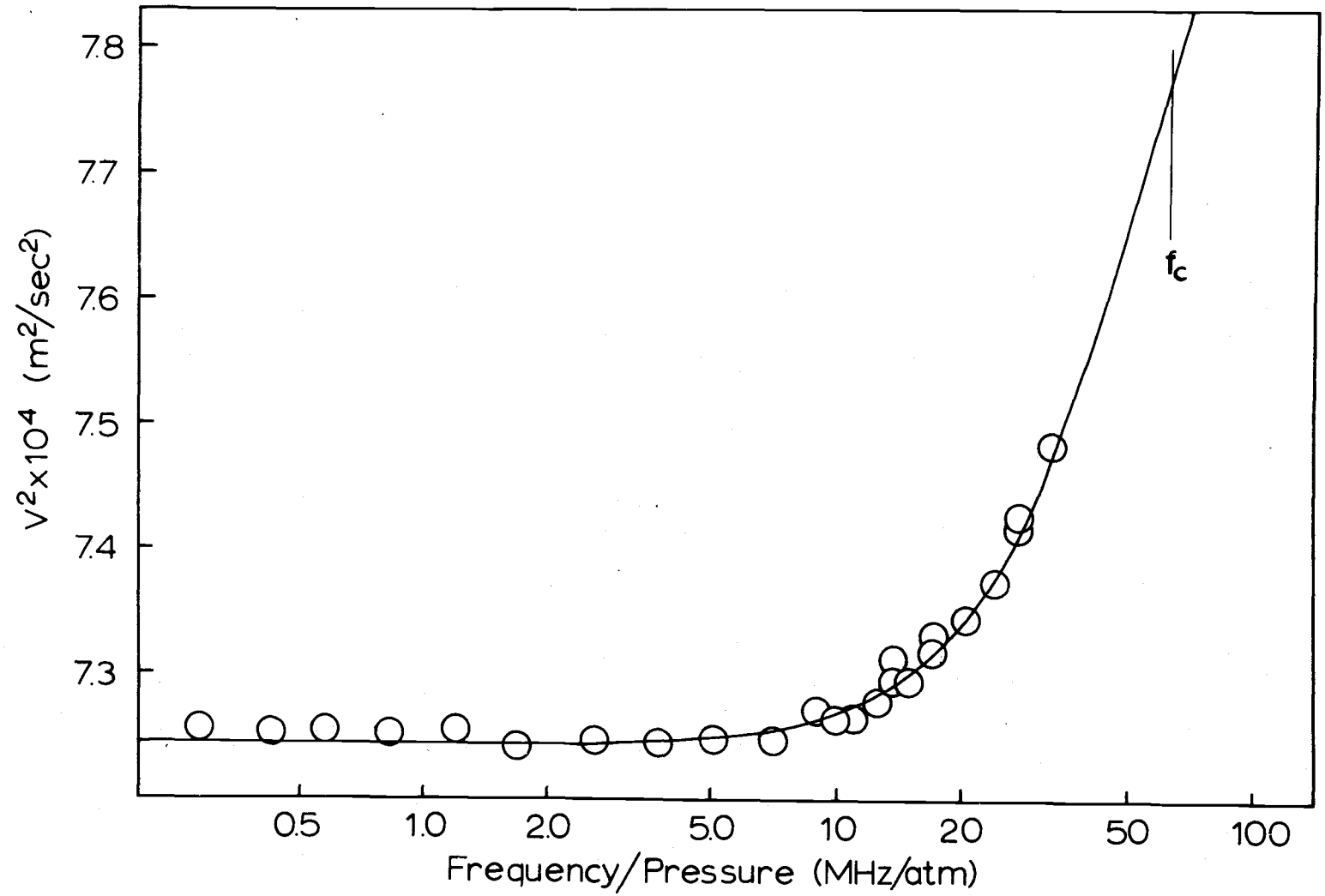


Figure 7. Ideal sound velocity in allene at 300°K.

would have the distinction of being the fastest vibrationally relaxing molecule reported in the literature.

The possibility that part of the velocity dispersion seen in Figure 7 could be due to translational effects has been considered, but a calculation of translational dispersion at 33 MHz/atm using equation (61) indicates an increase in velocity of only 0.025%.

A more serious problem is the effect of the impurities (0.6% propylene and 0.7% methyl acetylene) on the velocity data reported for allene. The relaxation time for propylene is $\tau = 1.5$ ns (43) which is some three to four times faster than allene. Methyl acetylene has not been investigated but would be expected to relax comparably to allene on the basis of their similar structure and lowest modes of vibration (328 $cm^{-1}$ for methyl acetylene versus 354 $cm^{-1}$ for allene). The role of catalyst molecules in promoting energy transfer is not well understood and there is a certain amount of conflicting literature on the subject. McCoubrey and coworkers (3, 45, 62) have extensively investigated the role of impurities on the vibrational relaxation times of polyatomic molecules. Their results indicate that additives exhibit the greatest catalytic effect on a sample gas under the following conditions.

i) The impurity has a much faster relaxation time than the sample gas.

ii) The impurity has a faster translational velocity, or, in the

classical sense, a faster rotational velocity.

iii) There is an enhanced attraction between the impurity and sample gas due to dipole moments or chemical affinity.

On the basis of the above criteria, one would not expect propylene or methyl acetylene to exert too great an influence on the vibrational relaxation time in allene. Indeed the observed value reported for allene agrees rather well with the Lambert Salter correlation (54) for molecules containing two or more hydrogen atoms.

The error introduced in the reported relaxation time for allene due to the presence of impurities can be estimated using equation (2.118) from Cottrell and McCoubrey (12, p. 32)

$$\frac{1}{\tau} = \frac{X_A}{\tau_{AA}} + \frac{X_B}{\tau_{AB}} \qquad (76)$$

In equation (76), $\tau$ is the experimentally observed relaxation time (for a gas composed mainly of A molecules with some B molecules), $\tau_{AA}$ is the relaxation time for the pure gas, A, and $\tau_{AB}$ is the relaxation time for a hypothetical gas in which only AB collisions occur. $X_A$ and $X_B$ are the respective mole fractions for gases A and B.

If we assume that for a gas composed of allene, propylene, and methyl acetylene, the most efficient transfer of vibrational-translational energy occurs during propylene-propylene collisions, equation

(76) may be solved to provide an error estimate. As an upper limit we set $\tau_{AB} = 1.5$ ns and $X_B = 0.013$; then from the observed relaxation time in allene, $\tau = 5.2$ ns, we can calculate the relaxation time for the pure gas, $\tau_{AA}$. Solving equation (76) gives $\tau_{AA} = 5.4$ ns. This indicates that impurities in the allene sample would be expected to decrease the relaxation time only by about four percent.

(4.3) Carbon Suboxide

Carbon suboxide has proven itself to be an interesting, if somewhat elusive, molecule to study. It is one of several which have a very low vibrational frequency; in this instance the bending of the central CCC group at 63 $cm^{-1}$ (68). The possibility of multiple relaxation exists as the next lowest vibrational frequency is at 550 $cm^{-1}$. This has been found to be the case and the longer of the two relaxation times has been determined to be $\tau_1 = 48$ ns. The 63 $cm^{-1}$ bend relaxes independently of the other vibrational modes at $\tau_2 < 1$ ns.

Until recently there has been some disagreement regarding the shape of the carbon suboxide molecule. The geometry has been interpreted as being both linear (57) and bent (85). As the two forms would be expected to possess differing heat capacities, very accurate measurement of this parameter should distinguish between the two structures. Unfortunately our heat capacity measurements on carbon suboxide are subject to some ambiguity due to the presence

of carbon dioxide impurity. This prevented an accurate comparison of the velocity limits of our sample with those predicted by statistical thermodynamics. It has now been fairly well established that carbon suboxide is linear (52). However, our velocity data, within the limitations just mentioned, appear to be about 0.5-1% higher than the theoretical value based on the linear interpretation. Election diffraction studies (1) indicate carbon suboxide is linear; but the molecule does show a large shrinkage effect which has been ascribed to the large mean amplitude of vibration about the central carbon atom.

Information regarding the chemical and physical properties of carbon suboxide may be found in a review article by Grauer (27).

## Experimental Data

The experimental study of carbon suboxide has proved difficult for a number of reasons. The synthesis of the compound has certain drawbacks and yields are correspondingly small. What product is obtained must be tediously fractionated to reduce the carbon dioxide impurity. At no time was there more than one to two liters of gas available for study. This meant that extreme care had to be practiced in order to insure the purity of the sample, which from necessity was used over and over many times. Carbon suboxide is also unstable and polymerizes rapidly at pressures much above 30-40 cm Hg. Long term storage can only be accomplished at liquid nitrogen

temperature.

Velocity measurements on carbon suboxide were performed over the range 1.1-22 MHz/atm using the 0.56 MHz crystal and 3.7-41 MHz/atm using the 1.07 MHz crystal. The sound velocities were calculated in the standard manner using equations (72), (73), and (75). Experimental data taken with the 1.07 MHz crystals are shown in Tables 7 and 8 and with the 0.56 MHz crystal in Tables 9 and 10. Real sound velocities were corrected to ideality using equation (47) and S = -550 cc/mole. The R. F. voltages applied to the crystals were in the range 85-200 volts. The exposure times for carbon suboxide are from 0.04-160 seconds for pressures from 0.50-0.026 atmospheres. Nitrogen was used as a standard gas with the exception of series (8-17-68#1) which was taken with argon. Exposure times varied from 0.5-15 seconds for the standard gas with pressures from 0.50-0.08 atmospheres.

Nitrogen is not ideally suited as a standard gas for carbon suboxide measurement. This is due to the large difference in molecular weights and hence diffraction angles between the two gases. This introduces a moderate but fortunately constant error in velocity measurements due to optical distortion in the lens system. The effect is especially noticeable when using the 1.07 MHz crystal where diffraction angles are the greatest. The nature of this correction has been tested independently by pairing together three

Table 7. Velocity of sound in nitrogen (1.07 MHz crystal).

| Plate Identification | Pressure (atm) | Temperature ($^{o}$K) | Frequency (KHz) | Diffraction Distance (mm) | $V_i^2$ ($\times 10^4$ m$^2$/sec$^2$) | $V_{real}^2$ ($\times 10^4$ m$^2$/sec$^2$) |
|---|---|---|---|---|---|---|
| 12-13-68 #1 | 0.291 | 299.51 | 1069.350 | 6.2488 | 12.4451 | 12.4475 |
| " | 0.207 | 299.63 | .349 | 6.2487 | 12.4501 | 12.4517 |
| " | 0.155 | 299.80 | .347 | 6.2440 | 12.4571 | 12.4583 |
| 12-9-68 #2 | 0.151 | 299.07 | 1069.372 | 6.2542 | 12.4268 | 12.4280 |
| " | 0.118 | 299.09 | .370 | 6.2598 | 12.4276 | 12.4286 |
| " | 0.118 | 299.05 | .370 | 6.2570 | 12.4260 | 12.4270 |
| 12-10-68 #1 | 0.103 | 299.22 | 1069.329 | 6.2458 | 12.4330 | 12.4339 |
| " | 0.103 | 299.26 | .327 | 6.2506 | 12.4347 | 12.4356 |
| " | 0.103 | 299.23 | .328 | 6.2508 | 12.4334 | 12.4343 |
| 12-10-68 #2 | 0.092 | 301.65 | 1069.299 | 6.2188 | 12.5340 | 12.5348 |
| " | 0.089 | 301.68 | .298 | 6.2120 | 12.5352 | 12.5360 |
| 12-10-68 #3 | 0.079 | 299.57 | .301 | 6.2397 | 12.4476 | 12.4482 |
| 2-5-69 #2 | 0.155 | 299.98 | 1069.302 | 6.2443 | 12.4646 | 12.4658 |
| " | 0.145 | 300.04 | .302 | 6.2418 | 12.4671 | 12.4682 |
| " | 0.132 | 300.04 | .303 | 6.2424 | 12.4671 | 12.4682 |
| 2-5-69 #1 | 0.117 | 300.10 | 1069.301 | 6.2414 | 12.4696 | 12.4706 |
| " | 0.105 | 300.14 | .301 | 6.2428 | 12.4713 | 12.4722 |
| " | 0.092 | 300.13 | .302 | 6.2381 | 12.4708 | 12.4715 |
| " | 0.079 | 300.19 | .301 | 6.2380 | 12.4733 | 12.4739 |

Table 8. Ideal velocity of sound in carbon suboxide (1.07 MHz crystal).

| Plate Identification | Pressure (atm) | Temperature ($^{o}$K) | Frequency (KHz) | Diffraction Distance (mm) | $V^2_{300^{o}K}$ ($\times 10^4$ $m^2/sec^2$) | $V_i^2$ ($\times 10^4$ $m^2/sec^2$) | f/P (MHz/atm) |
|---|---|---|---|---|---|---|---|
| 12-13-68 #1 | 0.290 | 299.76 | 1069.344 | 10.5366 | 4.3094 | 4.3670 | 3.69 |
| " | 0.208 | 299.72 | .344 | 10.4574 | 4.3779 | 4.4194 | 5.14 |
| " | 0.154 | 299.76 | .343 | 10.3962 | 4.4256 | 4.4568 | 6.95 |
| 12-9-68 #2 | 0.118 | 297.51 | 1069.369 | 10.3906 | 4.4681 | 4.4924 | 9.03 |
| " | 0.095 | 297.49 | .369 | 10.3658 | 4.4986 | 4.5185 | 11.3 |
| " | 0.078 | 297.29 | .369 | 10.3505 | 4.5106 | 4.5264 | 13.8 |
| 12-10-68 #1 | 0.066 | 300.72 | 1069.304 | 10.2577 | 4.5266 | 4.5402 | 16.2 |
| " | 0.053 | 300.87 | .305 | 10.2432 | 4.5450 | 4.5564 | 20.3 |
| " | 0.044 | 300.98 | .302 | 10.2247 | 4.5600 | 4.5691 | 24.2 |
| " | 0.038 | 301.30 | 1069.298 | 10.2064 | 4.5614 | 4.5696 | 28.0 |
| " | 0.033 | 301.75 | .287 | 10.1774 | 4.5712 | 4.5781 | 32.5 |
| 12-10-68 #3 | 0.026 | 299.55 | .290 | 10.2195 | 4.5754 | 4.5809 | 40.7 |
| 2-5-69 #2 | 0.114 | 300.75 | 1069.302 | 10.3438 | 4.4595 | 4.4806 | 9.34 |
| " | 0.101 | 300.72 | .301 | 10.3206 | 4.4776 | 4.4965 | 10.6 |
| " | 0.082 | 300.66 | .300 | 10.3024 | 4.4955 | 4.5108 | 13.3 |
| 2-5-69 #1 | 0.066 | 300.20 | 1069.303 | 10.2982 | 4.5056 | 4.5178 | 16.2 |
| " | 0.049 | 300.75 | .300 | 10.2694 | 4.5256 | 4.5347 | 22.0 |
| " | 0.034 | 300.78 | .299 | 10.2534 | 4.5322 | 4.5386 | 31.3 |
| " | 0.026 | 300.63 | .301 | 10.2516 | 4.5369 | 4.5419 | 40.7 |

Table 9. Velocity of sound in nitrogen (0.56 MHz crystal).

| Plate Identification | Pressure (atm) | Temperature ($^{o}$K) | Frequency (KHz) | Diffraction Distance (mm) | $V_i^2$ ($\times 10^4$ m$^2$/sec$^2$) | $V_{real}^2$ ($\times 10^4$ m$^2$/sec$^2$) |
|---|---|---|---|---|---|---|
| 12-18-68 #1 | 0.497 | 299.92 | 558.218 | 3.2608 | 12.4621 | 12.4661 |
| " | 0.447 | 299.96 | .218 | 3.2630 | 12.4638 | 12.4674 |
| " | 0.394 | 299.96 | .219 | 3.2634 | 12.4638 | 12.4669 |
| 12-17-68 #1 | 0.290 | 299.56 | 560.665 | 3.2764 | 12.4472 | 12.4496 |
| " | 0.236 | 299.66 | .664 | 3.2814 | 12.4513 | 12.4532 |
| " | 0.185 | 299.77 | .706 | 3.2840 | 12.4559 | 12.4574 |
| 12-17-68 #2 | 0.342 | 299.84 | 558.216 | 3.2628 | 12.4588 | 12.4615 |
| " | 0.134 | 299.97 | .207 | 3.2628 | 12.4642 | 12.4653 |
| 8-17-68 #1 (Argon) | 0.258 | 300.53 | 559.738 | 3.6060 | 10.4248 | 10.4262 |
| " | 0.207 | 300.52 | .737 | 3.6043 | 10.4245 | 10.4256 |
| " | 0.170 | 300.55 | .733 | 3.6040 | 10.4255 | 10.4264 |
| 8-16-68 #1 | 0.125 | 299.80 | 559.747 | 3.2880 | 12.4571 | 12.4581 |
| " | 0.125 | 299.82 | .747 | 3.2875 | 12.4580 | 12.4590 |
| " | 0.125 | 299.83 | .747 | 3.2876 | 12.4584 | 12.4594 |
| " | 0.125 | 299.85 | .748 | 3.2867 | 12.4592 | 12.4602 |
| " | 0.125 | 299.86 | .748 | 3.2868 | 12.4596 | 12.4606 |
| 8-15-68 #1 | 0.094 | 300.35 | 559.769 | 3.2812 | 12.4800 | 12.4807 |
| 8-16-68 #2 | 0.143 | 300.77 | 559.738 | 3.2906 | 12.4974 | 12.4985 |
| " | 0.143 | 300.77 | .738 | 3.2894 | 12.4974 | 12.4985 |
| " | 0.143 | 300.77 | .738 | 3.2909 | 12.4974 | 12.4985 |
| " | 0.143 | 300.78 | .738 | 3.2902 | 12.4979 | 12.4990 |
| " | 0.143 | 300.78 | .739 | 3.2911 | 12.4979 | 12.4990 |

Table 10. Ideal velocity of sound in carbon suboxide (0.56 MHz crystal).

| Plate Identification | Pressure (atm) | Temperature ($^{o}$K) | Frequency (KHz) | Diffraction Distance (mm) | $V^2_{300^{o}K}$ ($\times 10^4$ $m^2/sec^2$) | $V_i^2$ ($\times 10^4$ $m^2/sec^2$) | f/P (MHz/atm) |
|---|---|---|---|---|---|---|---|
| 12-18-68 #1 | 0.496 | 299.81 | 558.223 | 5.6201 | 4.1992 | 4.2954 | 1.12 |
| " | 0.447 | 299.77 | .219 | 5.6210 | 4.2045 | 4.2907 | 1.25 |
| " | 0.395 | 299.74 | .218 | 5.6126 | 4.2184 | 4.2948 | 1.41 |
| 12-17-68 #1 | 0.287 | 299.94 | 560.703 | 5.6077 | 4.2513 | 4.3073 | 1.96 |
| " | 0.236 | 299.96 | .703 | 5.5910 | 4.2908 | 4.3372 | 2.37 |
| " | 0.183 | 299.97 | .718 | 5.5634 | 4.3412 | 4.3775 | 3.07 |
| 12-17-68 #1 | 0.339 | 299.65 | 558.219 | 5.5948 | 4.2431 | 4.3095 | 1.65 |
| " | 0.130 | 299.70 | .220 | 5.5002 | 4.3912 | 4.4173 | 4.28 |
| 8-17-68 #1 | 0.258 | 300.58 | 559.737 | 5.6010 | 4.2832 | 4.3339 | 2.17 |
| " | 0.206 | 300.53 | .738 | 5.6206 | 4.3097 | 4.3502 | 2.72 |
| " | 0.171 | 300.53 | .737 | 5.5814 | 4.3396 | 4.3737 | 3.27 |
| 8-16-68 #1 | 0.124 | 300.54 | 599.744 | 5.5424 | 4.3752 | 4.4003 | 4.51 |
| " | 0.092 | 300.54 | .744 | 5.5068 | 4.4320 | 4.4511 | 6.06 |
| " | 0.069 | 300.50 | .746 | 5.4784 | 4.4786 | 4.4930 | 8.07 |
| " | 0.057 | 300.46 | .748 | 5.4674 | 4.4972 | 4.5089 | 9.80 |
| " | 0.046 | 300.41 | .748 | 5.4572 | 4.5148 | 4.5243 | 12.1 |
| 8-15-68 #1 | 0.067 | 300.07 | 559.760 | 5.4754 | 4.4808 | 4.4943 | 8.38 |
| 8-16-68 #2 | 0.123 | 300.78 | 559.740 | 5.5427 | 4.3938 | 4.4185 | 4.55 |
| " | 0.070 | 300.79 | .738 | 5.4815 | 4.4918 | 4.5062 | 8.06 |
| " | 0.045 | 300.75 | .740 | 5.4580 | 4.5312 | 4.5407 | 12.4 |
| " | 0.030 | 300.70 | .741 | 5.4490 | 4.5469 | 4.5533 | 18.8 |
| " | 0.025 | 300.65 | .741 | 5.4434 | 4.5570 | 4.5625 | 22.6 |

different standard gases; Kr, Ar, and $N_2$, using both the 0.56 MHz and 1.07 MHz crystals. Real sound velocities squared in carbon suboxide have been semi-empirically corrected for optical distortion by subtracting $0.072 \times 10^4$ $m^2/sec^2$ from measurements obtained using the 1.07 MHz crystal.

Experimental Results

Sound velocity measurements in carbon suboxide, shown in Figure 8, reveal a multiple relaxation process with all of the vibrational modes, except the bend $\nu_7 = 63$ $cm^{-1}$, relaxing together at $\tau_1 = 48$ ns.

Ideal sound velocities in carbon suboxide have been calculated for 300°K using vibrational heat capacities based on the spectroscopic data of Miller and Fateley (67) and Miller, Lemmon and Witkowski (68). The normal modes of vibration and their contribution to the heat capacity are listed in Table 11. The values of the heat capacity predicted by statistical thermodynamics are $C_v = 7.078R$ under static conditions, $4.485R$ after the loss of all modes except $\nu_7$, and $2.500R$ with just the external degrees of freedom excited. The theoretical velocity limits corresponding to the above heat capacities are

$V_o^2 = 4.1845 \times 10^4$ $m^2/sec^2$ static velocity

$V_m^2 = 4.4841 \times 10^4$ $m^2/sec^2$ all modes except $\nu_7$ relaxing

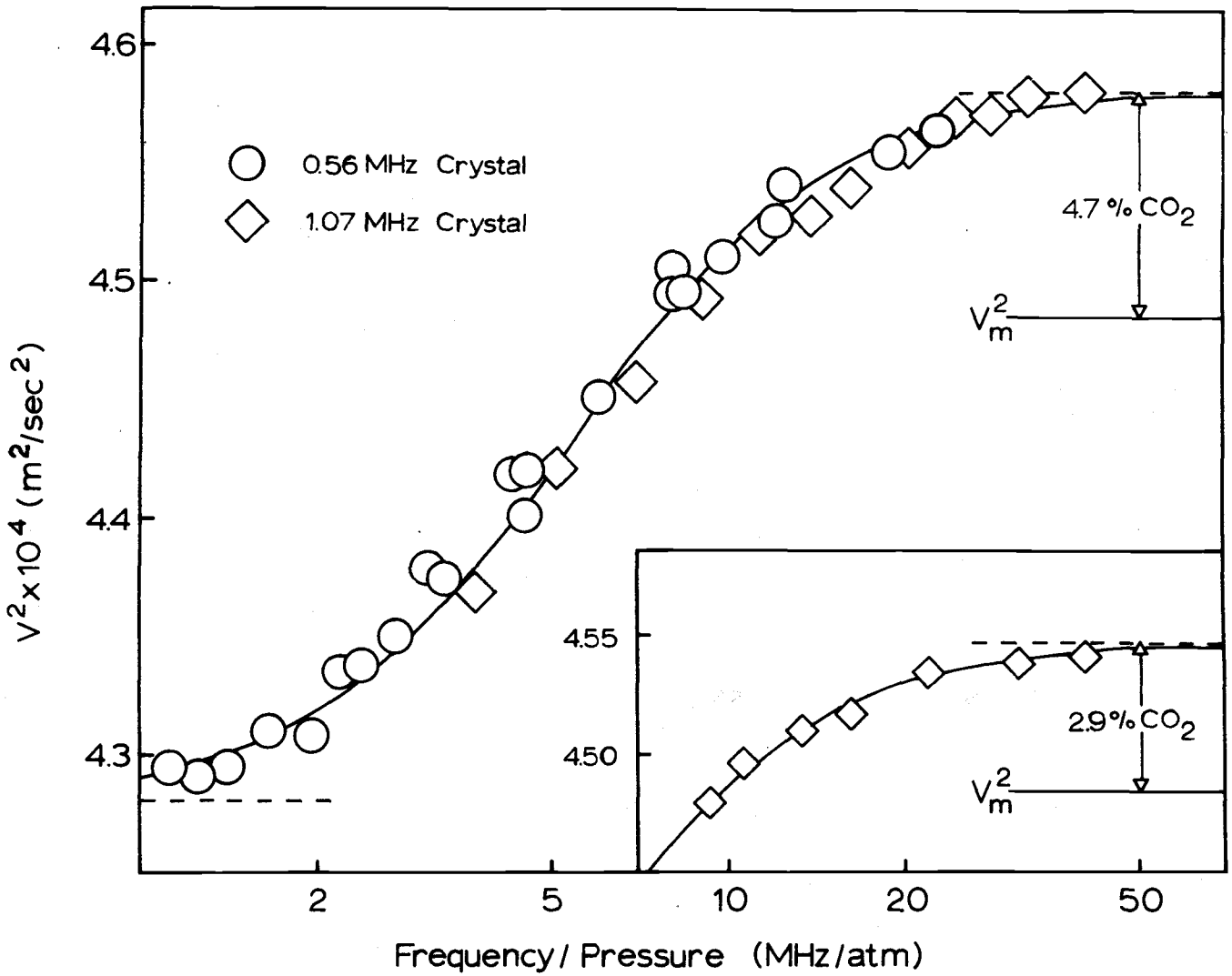


Figure 8. Ideal sound velocity in carbon suboxide samples at 300°K.

Table 11. The vibrational heat capacity of carbon suboxide at 300°K.

| Vibration | Frequency $cm^{-1}$ | $C_v/R$ |
|---|---|---|
| $\nu_7(E)$ | 63 | 1.9848 |
| $\nu_6(E)$ | 550 | 1.1544 |
| $\nu_5(E)$ | 577 | 1.0958 |
| $\nu_2$ | 830 | 0.3074 |
| $\nu_4$ | 1573 | 0.0302 |
| $\nu_1$ | 2200 | 0.0031 |
| $\nu_3$ | 2258 | 0.0024 |

Vibrational Total $C_v/R = 4.5781$

$V_{\infty}^2 = 5.1331 \times 10^4 \ m^2/sec^2$ high frequency velocity

where $V_o^2$, and $V_{\infty}^2$ have been defined in equations (37) and (38) and $V_m^2$ is the intermediate limiting velocity should the separation of the two relaxation processes be complete.

The dispersion curve which fits the velocity data in Figure 8 has been calculated using equation (36) with $C_o = 7.078R$ and $C_{\infty} = 4.485R$. The velocities reported are bulk measurements, and are seen to be higher than the predicted limiting velocity, $V_m^2$, by an amount corresponding to 4.7% $CO_2$ impurity.

The correction of the observed sound velocity of the impure carbon suboxide sample was carried out on the assumption that both M and $C_v$ in the formula

$$V_i^2 = \frac{RT}{M}\left(1+\frac{R}{C_v}\right) \tag{34}$$

should be expressed as mole weighted averages

$$M = (1-X)\,M_A + X\,M_B \tag{77a}$$

$$C_v = (1-X)C_A + X\,C_{vB} \tag{77b}$$

where X is the mole fraction of carbon dioxide and the subscripts A and B refer respectively to carbon suboxide and carbon dioxide.

For relatively small impurities, it is found that the percentage velocity correction is roughly 1/2 the percentage carbon dioxide

impurity. The lower mass of carbon dioxide dominates the correction, and causes the impure gas to have a higher velocity than that of pure carbon suboxide.

Study of the carbon suboxide sample by mass spectrometer and infrared analysis does not accurately fix the carbon dioxide content, but suggests a carbon dioxide level of 3 ± 1 mole percent. On the other hand, agreement of the experimental asymptotic value, $V_m^2$, with theory requires the assumption of 4.7% impurity. Alternately, should the carbon suboxide molecule be bent rather than linear, the reassignment of the specific heat could feasibly account for the observed discrepancy.

In order to confirm that the difference in experimental and theoretical velocity limits is due, at least in part, to carbon dioxide impurity, additional velocity measurements were performed on a more pure sample. The carbon suboxide sample being used in the investigation was vacuum fractionated to 1/4 of its original size. The total pressure attainable when this small amount of carbon suboxide was introduced into the apparatus was only 0.11 atm and accordingly the velocity data extend over a small range, 9.3-41 MHz/atm. Great care was taken to introduce a uniform sample into the system so that the tendency for carbon dioxide to vaporize first would not affect the results. The velocities obtained are of high precision and are shown in the inset in Figure 8. A decrease in

velocity has been noted corresponding to a sample containing 97.1% $C_3O_2$ and 2.9% $CO_2$. These data points in particular are quite convincing that the beginning of the second vibrational relaxation step, corresponding to the loss of $\nu_7$, has not yet begun.

The catalytic effect of carbon dioxide on the relaxation of carbon suboxide appears to be slight. The carbon suboxide sample shown in the inset gives a slightly longer relaxation time, $\tau_1 = 50$ ns. If this difference can be regarded as significant, then by linear extrapolation, the relaxation time in pure carbon suboxide would be between 53-54 ns.

An upper limit for the relaxation of the 63 $cm^{-1}$ bend may be estimated using the multiple dispersion equation. The velocity curve shown in Figure 9 has been calculated from equation (41) using $C_o = 7.078R$, $C_1 = 2.593R$, $C_2 = 1.985R$, $C_\infty = 2.500R$, $\tau_1 = 48$ ns, and $\tau_2 = 1.0$ ns. The velocity component due to the presence of carbon dioxide has been subtracted out using equations (77ab) with the mole fraction, $X = 0.047$, varying about 20% to account for carbon dioxide's preferential vapor pressure. Mass spectrum analysis of several carbon suboxide samples indicated that the low pressure samples were about 20% richer in carbon dioxide than high pressure measurements. The vapor pressure correction tends to decrease the nonideality parameter, and the value $S = -490$ cc/mole is based on the best fit of carbon suboxide data at two different crystal

frequencies.

On the basis of the dotted portion of the double dispersion curve in Figure 9, corresponding to $\tau_2 = 1.0$ ns, we conclude the relaxation of the $\nu_7$ mode in carbon suboxide is equal to or less than one nanosecond.

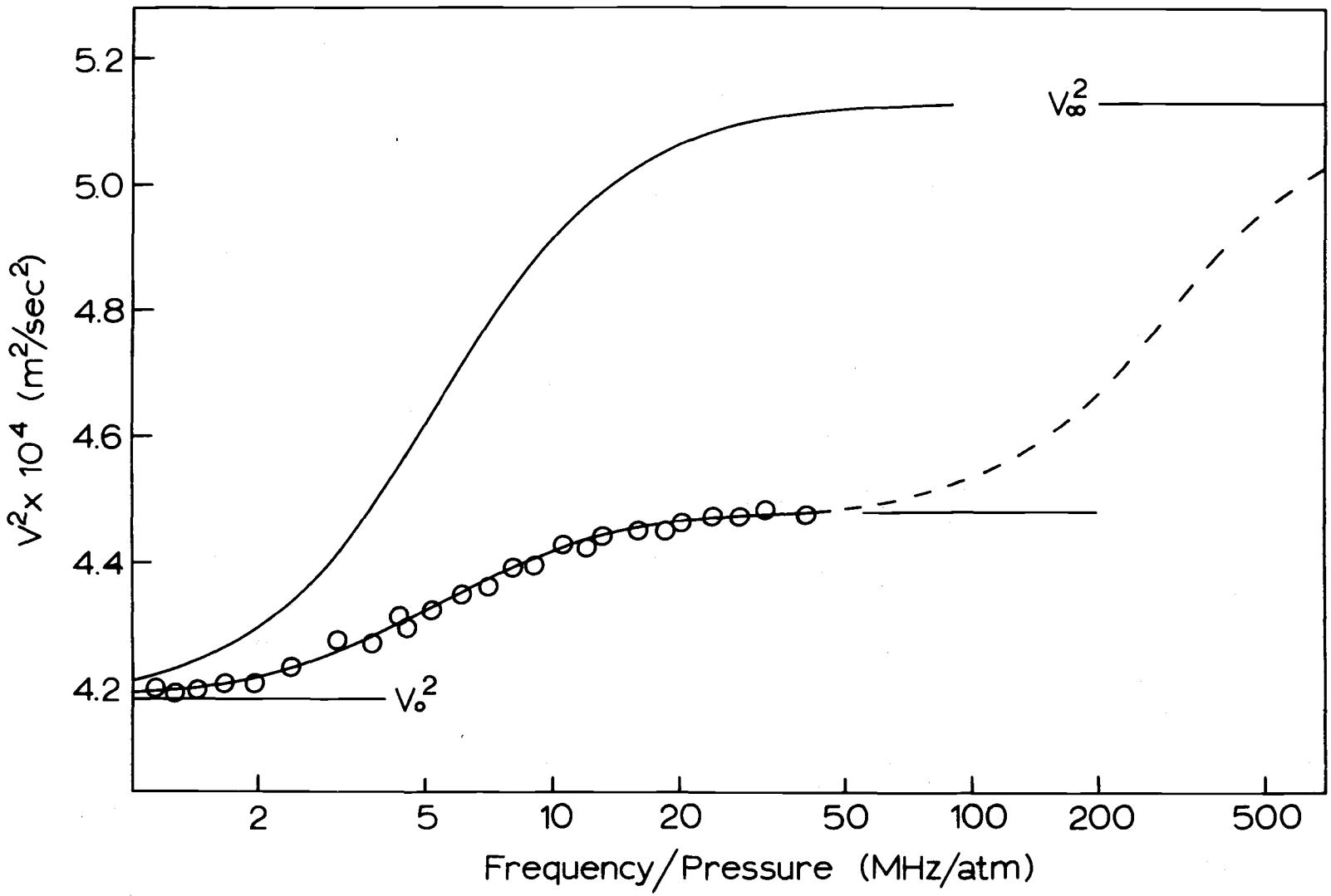


Figure 9. Observation of multiple relaxation in carbon suboxide.

## DISCUSSION OF MULTIPLE RELAXATION

Polyatomic molecules generally exhibit a single vibrational relaxation time associated with all of the vibrational specific heat of the molecule. The rate determining step is with few exceptions (101) the transfer of energy between the lowest vibrational mode and the external degrees of freedom. For the few molecules where there is a large frequency discrepancy between modes, the transfer of energy through such modes may also prove to be a rate determining step. In these instances, multiple relaxation would be expected to occur. This has been observed in only a few gases to date; namely $SO_2$ (53, 62, 94), $C_2H_6$ (2, 43, 54, 106), $CH_2Cl_2$ (91), $CH_2Br_2$ (32, 66), and in the present investigation $C_3O_2$ (35, 36). In each of these molecules there is a large energy gap between the lowest and the second lowest fundamental modes of vibration.

A summary of gases in which multiple relaxation processes are known to occur is presented in Table 12. Also listed are molecules which have been reported to be singly relaxing, but appear to have the same qualifications found in molecules exhibiting multiple relaxation. That this table is amazingly small is a result of the rapid processes of vibrational-vibrational energy transfer which occur during molecular encounters. Collision numbers rather than relaxation times are reported in Table 12 as these data are more meaningful

Table 12. Room temperature collision numbers for molecules expected to exhibit double dispersion.

| Compound | $\nu$ (1) | $\nu$ (2) | i | $\Delta\nu$ | $Z_{21}$ | $Z_{10}$ | Reference |
|---|---|---|---|---|---|---|---|
| $SO_2$ | 519 | 1151 | 2 | 113 | 7480 | 520 | McCoubrey (62) |
| | | | | | 2380 | 330 | Lambert (53) |
| $CH_2Cl_2$ | 283 | 704 | 2 | 138 | 450 | 23 | Sette (91) |
| $CH_2Br_2$ | 174 | 576 | 3 | 54 | ? | ? | Meyer (66) |
| $C_2H_6$ | 289 | 821 | 3 | ? | 100 | 16 | Valley (107) |
| | | | | | 92 | 10 | Holmes (43) |
| | | | | | 74 | 20 | Lambert (54) |
| $C_3O_2$ | 63 | 550 | 9 | -17 | 460 | $\lesssim 3$ | this work |
| $C_3H_4$ | 354 | 842 | 2 | 134 | -- | 33 | this work |
| $CH_3OH$ | 335 | 1030 | 3 | 35 | -- | 7 | Ener (23) |
| $CH_2{=}CHCH_3$ | 177 | 417 | 2 | ? | -- | 6 | Holmes (43) |

from a comparative as well as a theoretical point of view. The collision number, $Z_{10}$, is defined as the average number of collisions necessary to transfer one quantum of vibrational energy from the ground to the lowest excited vibrational state in a molecule. $Z_{21}$ is the number of collisions associated with the exchange of vibrational energy between the lowest and second lowest vibrational modes, $\nu(1)$ and $\nu(2)$. These values have been calculated from experimental relaxation times using a modified form of expression (43), which applies to a singly relaxing gas, and are shown in equations (78) and (79).

$$Z_{21} = Z \tau_1 C_2^{vib} \left[ \sum_{j=2}^{3n-6} C_j^{vib} \right]^{-1} \left[ 1 - \exp \left( -\frac{h\nu(2)}{kT} \right) \right] \tag{78}$$

$$Z_{10} = Z \tau_2 \left[ 1 - \exp \left( -\frac{h\nu(1)}{kT} \right) \right] \tag{79}$$

where $C_2^{vib}$ is the heat capacity of the second lowest vibrational mode and the other terms are as defined previously. In the case of carbon suboxide, the heat capacity term, $C_2^{vib}$, has been modified to include both modes $\nu_6$ and $\nu_5$ at 550 $cm^{-1}$ and 577 $cm^{-1}$ since they are close enough to both to be effective in transferring energy to the $\nu_7 = 63$ $cm^{-1}$ vibration. Calculation of Z, the number of collisions per molecule per second, is based on the rigid sphere model (equation (44)) for all molecules listed with the exception of $C_3H_4$

and $C_3O_2$. For $C_3H_4$, where Lennard Jones parameters are available, Z was calculated using equation (5.6) of Cottrell and McCoubry (12, p. 75). The value for $C_3O_2$ was estimated using the Z obtained from $C_3H_4$ taking into account their difference in masses.

In Table 12, $\Delta\nu$ refers to the energy discrepancy for kinetic reactions involving transfer of vibrational energy from the second lowest mode to an overtone of the first; hence $\Delta\nu = \nu(2) - i\nu(1)$, i = 2, 3, ... For molecules such as ethane and propylene in which the lowest mode is the hindered internal rotation, the potential function describing the torsional oscillation is very anharmonic and $\Delta\nu$ is not well known, although one could use the restricted rotor model and, for example, the data of Weiss and Leroi (108).

Collisional deactivation numbers for $CH_2Br_2$ have not been listed in Table 12 as this molecule has been interpreted by Meyer (66) and again by Hageseth (32) to be triply dispersive. The modal assignment associated with these three relaxation times, based entirely on experimental specific heats, is:

$\tau_1$ = 4600 nanoseconds ($\nu$ = 576, 1091, 1183 $cm^{-1}$)

$\tau_2$ = 30 nanoseconds ($\nu$ = 174, 810, 1388 $cm^{-1}$)

$\tau_3$ = 1.5 nanoseconds ($\nu$ = 637 $cm^{-1}$)

This assignment is most probably incorrect. It is interesting to note that two modes only 61 $cm^{-1}$ apart ($\nu_2$ = 576 and $\nu_9$ = 637 $cm^{-1}$) are

reported to have relaxation times of 4600 ns and 1.5 ns respectively. Such a separation is very unlikely if not impossible. Although the experimental data presented by Meyer and Hageseth indicate that more than a single relaxation process is occurring, the data are not sufficiently accurate to justify the empirical assignments these authors presented, especially in view of the current theoretical interpretation of multiple vibrational relaxation.

To date, theoretical studies of multiple relaxation in gases have been based entirely on the method of Schwartz, Slawsky, and Herzfeld (88, 89). Tanzos (103) in extending the SSH method to polyatomic molecules predicted double dispersion in $CH_2Cl_2$ in accord with the experimental work of Sette, Busala and Hubbard (91). In calculating the rate of deactivation of the vibrational energy of a particular mode, Tanzos considered complex collisions involving total changes of up to three quanta. His results indicated that $CH_2Cl_2$ should be doubly relaxing with the second and all higher modes associated with the slower process, and the lowest mode associated with the high frequency relaxation. The rate determining step for $CH_2Cl_2$ is a three quantum process in which the CCl stretching vibration $\nu_3 = 704\ cm^{-1}$ transfers one quantum of vibrational energy to the first overtone of the $CCl_2$ bend $\nu_4 = 283\ cm^{-1}$, the excess energy being taken up by the translational motion

$$CH_2Cl_2(\nu_3) + CH_2Cl_2 \rightarrow CH_2Cl_2\,(2\nu_4) + CH_2Cl_2 + 138\ cm^{-1} \quad (80)$$

A similar calculation carried out by Dickens and Linnett (21) on $SO_2$ indicates the same pattern; the rate determining step being the transfer of vibrational energy from the symmetric stretching vibration $\nu_1 = 1151\ cm^{-1}$ to the first overtone of the bend $\nu_2 = 521\ cm^{-1}$.

$$SO_2(\nu_1) + SO_2 \rightarrow SO_2(2\nu_2) + SO_2 + 113\ cm^{-1} \quad (81)$$

These results also agree with the experimental data (53, 62).

Dickens and Schofield (22), noting Meyer's unusual report of three relaxation times in $CH_2Br_2$ performed an SSH calculation on this molecule with the now anticipated results. Double dispersion was predicted with the lowest mode relaxing independently of the rest, and the rate determining step for the slower process being the deactivation of the second lowest vibrational mode to the lowest. Although their calculations are extended to take into account transitions involving up to four vibrational quanta, it is not stated whether the rate determining step is transfer to the ground state, or the first or second overtone of the $\nu_4 = 174\ cm^{-1}$ vibration.

$$CH_2Br_2(\nu_2) + CH_2Br_2 \rightarrow CH_2Br_2(3\nu_4) + CH_2Br_2 + 54\ cm^{-1} \quad (82a)$$

$$CH_2Br_2(\nu_2) + CH_2Br_2 \rightarrow CH_2Br_2(2\nu_4) + CH_2Br_2 + 228\ cm^{-1} \quad (82b)$$

$$CH_2Br_2(\nu_2) + CH_2Br_2 \rightarrow CH_2Br_2(\nu_4) + CH_2Br_2 + 402\ cm^{-1} \quad (82c)$$

Although the SSH method does not yield well defined selection rules for vibrational energy exchange during collisions, the method does predict two trends that are well established.

(i) The probability for energy transfer to occur increases as less energy must be transferred into translation.

(ii) The probability for energy transfer to occur decreases as more vibrational quantum number changes are required.

The kinetic expressions for $CH_2Br_2$ listed in equations (82a, b, c) show how these two trends tend to oppose each other in promoting energy transfer between the vibrational level of one mode and the overtone level of a second, much lower mode.

The $C_3O_2$ molecule represents an extreme case of this situation. The transfer of vibrational energy between the two bending vibrations $\nu_6 = 550\ cm^{-1}$ and $\nu_7 = 63\ cm^{-1}$ may be represented by nine equations

$$C_3O_2(\nu_6) + C_3O_2 \rightarrow C_3O_2(9\nu_7) + C_3O_2 - 17\ cm^{-1} \quad (83a)$$

$$C_3O_2(\nu_6) + C_3O_2 \rightarrow C_3O_2(8\nu_7) + C_3O_2 + 46\ cm^{-1} \quad (83b)$$

$$\text{-------} \quad \text{-----} \quad \text{--------} \quad \text{-----} \quad \text{-------} \quad \text{----}$$

$$C_3O_2(\nu_6) + C_3O_2 \rightarrow C_3O_2(\nu_7) + C_3O_2 + 487\ cm^{-1} \quad (83i)$$

Equation (83a) is a 10 quantum process and is expected to have

a very small transition probability. To see this effect one need look only at the matrix element of the perturbation $V_{kl}$ which must be nonzero during the encounter. In order for the vibrational integral to be nonzero, one term in $V_{kl}$ must contain each vibrational coordinate whose quantum number is changed, raised to the power of the quantum number change. Hence for process (83a) we need a term $F_{19}\ (q_{bend})\ (q'_{bend})^9$. However, since such terms become rapidly small for increasing powers of the vibrational coordinate we would expect the $F_{19}$ contribution to be very small indeed. Contrast this with equation (83i) which would be represented by a matrix element $F_{11}\ (q_{bend})\ (q'_{bend})$. A priori we would expect neither equation (83a) nor (83i) to be the most favorable transition path. Unfortunately a theoretical evaluation of these kinetic equations would be a most difficult task since angle dependent collisions summed over each atom would have to be considered.

Despite the success of the SSH theory and the apparent similarity between gases exhibiting multiple relaxation, the prospect of reliably predicting such behavior either theoretically or empirically is still not completely satisfactory. The trend is always that more gases are predicted to be doubly relaxing than actually is found to be the case. Tanzos (103), for example, finds the SSH method predicts $CHCl_3$ and $CCl_4$ should also exhibit two major relaxation times whereas only single relaxation processes have been observed

experimentally (91). An empirical rule of thumb states that for molecules in which the second lowest vibrational frequency is more than twice that of the lowest, double relaxation is expected. However as shown in Table 12, allene, propylene, and methanol meet these requirements but are singly dispersive.

Basic to an understanding of multiple relaxation is knowledge regarding the rates of intramolecular and intermolecular energy transfer in gases. These areas are just presently being investigated.

# BIBLIOGRAPHY


1. Almenningen, A., S. P. Arnesen, O. Bastiansen, H. M. Seip and R. Seip. The effect of temperature variation on the amplitudes of vibration and shrinkage effects in carbon suboxide studied by gas electron diffraction. Chemical Physics Letters 1:569-574. 1968.

2. Amme, R. C. and B. E. Warren. Ultrasonic velocity dispersion in ethane-argon mixtures. Journal of the Acoustical Society of America 44:419-422. 1968.

3. Arnold, J. W., J. C. McCoubrey and A. R. Ubbelohde. Efficiencies of additives in the transfer of vibrational energy in ethylene and nitrous oxide. Proceedings of the Royal Society (London), ser. A, 248:445-459. 1958.

4. Bergmann, Ludwig. Der Ultraschall und seine Anwendung in Wissenschaft und Technik. 6th ed. Stuttgart, S. Hirzel, 1954. 1114 p.

5. Berry, M. V. The diffraction of light by ultrasound. New York, Academic, 1966. 143 p.

6. Born, Max and Emil Wolf. Principles of optics. 3d ed. New York, Pergamon, 1965. 808 p.

7. Boyer, R. A. Translational dispersion in monatomic gases. Journal of the Acoustical Society of America 24:716-717. 1952.

8. Breshears, W. D. and P. F. Bird. Densitometric measurement of the vibrational relaxation of HCl and DCl in shock waves. The Journal of Chemical Physics 50:333-336. 1969.

9. _____ Vibrational relaxation of hydrogen halides. D Br and DI. The Journal of Chemical Physics, 1969. (In press)

10. Brillouin, Léon. Diffusion de la lumière et les rayons X par un corps transparent homogène influencé de l'agitation thermique. Annales de Physique 17:88-122. 1922.

11. Cottrell, T. L., R. C. Dobbie, J. McLain and A. W. Read. Transition probabilities in molecular encounters. Part VII. Further evidence for vibrational-rotational energy transfer. Relaxation in $AsH_3$ and $AsD_3$. Transactions of the Faraday Society 60:241-247. 1964.

12. Cottrell, T. L. and J. C. Mc Coubrey. Molecular energy transfer in gases. London, Butterworths, 1961. 205 p.

13. Cottrell, T. L., I. M. Mac Farlane and A. W. Read. Gas imperfection in ammonia and hydrogen cyanide determined by an ultrasonic method. Transactions of the Faraday Society 61:1632-1636. 1965.

14. Cottrell, T. L., I. M. Mac Farlane, A. W. Read and A. H. Young. Measurement of vibrational relaxation times by the spectrophone. Transactions of the Faraday Society 62:2655-2666. 1966.

15. Cottrell, T. L. and A. J. Matheson. Transition probability in molecular encounters. Part V. Vibrational-rotational energy transfer. Transactions of the Faraday Society 58: 2336-2341. 1962.

16. _____ Transition probability in molecular encounters. Part VI. Vibrational relaxation in $NH_3$, $ND_3$, $PH_3$ and $PD_3$. Transactions of the Faraday Society 59:824-829. 1963.

17. David, Erwin. Intensitatsformeln zur Lichtbengung an schwachen Ultraschallwellen. Physikalische Zeitschrift 38:587-591. 1937.

18. Debye, P. and R. W. Sears. On the scattering of light by supersonic waves. Proceedings of the National Academy of Sciences 18:409-414. 1932.

19. Decius, J. C. The diffraction of light by ultrasound in gases. Unpublished research. Corvallis, Oregon, Oregon State University, Dept. of Chemistry, 1968.

20. Dennison, D. M. The infrared spectra of polyatomic molecules. Part II. Reviews of Modern Physics 12:175-214. 1940.

21. Dickens, P. G. and T. W. Linnett. Calculation of vibrational relaxation times in gaseous sulfur dioxide. Proceedings of the Royal Society 243A:84-93. 1957.

22. Dickens, P. G. and D. Schofield. Multiple vibrational relaxation in gaseous dibromomethane. The Journal of Chemical Physics 35:374-375. 1961.

23. Ener, C., A. Busala and J. C. Hubbard. Ultrasonic dispersion in methyl alcohol vapor. The Journal of Chemical Physics 23:155-158. 1955.

24. Flygare, W. H., Professor, University of Illinois, Dept. of Chemistry. Personal correspondence. Urbana. March 26, 1969.

25. Gallant, R. W. Physical properties of hydrocarbons. Part IV. $C_2$ to $C_4$ diolefins. Hydrocarbon Processing and Petroleum Refiner 44(10):151-156. 1965.

26. Gaydon, A. G. and I. R. Hurle. The shock tube in high-temperature chemical physics. New York, Reinhold, 1963. 307 p.

27. Graver, Rolf. Das Kohlensuboxyd. Chimia 14:11-16. 1960.

28. Greenspan, Martin. Propagation of sound in five monatomic gases. Journal of the Acoustical Society of America 28:644-648. 1956.

29. _____ Rotational relaxation in nitrogen, oxygen and air. Journal of the Acoustical Society of America 31:155-160. 1959.

30. Griesbaum, K. Progress in the chemistry of allene. Angewandte Chemie. (International Edition in English) 5:933-946. 1966.

31. Haar, Lester. Thermodynamic properties of ammonia as an ideal gas. Journal of Research of the National Bureau of Standards 72A:207-216. 1968.

32. Hageseth, G. J. Multiple relaxation in gaseous dibromomethane. Journal of the Acoustical Society of America 42: 844-847. 1967.

33. Hamada, K. and Y. Fujii. Ultrasonic attenuation and relaxation times in water vapor and heavy-water vapor. Journal of the Acoustical Society of America 39:250-254. 1966.

34. Hamann, S. D., W. J. Mc Namey and J. F. Pearse. The forces between polyatomic molecules. Transactions of the Faraday Society 49:351-357. 1953.

35. Hancock, J. K. and J. C. Decius. Sound velocity in carbon suboxide. Science 164:587-588. 1969.

36. _____ Ultrasonic dispersion observed by optical diffraction. III. Allene and carbon suboxide. The Journal of Chemical Physics, 1970. (In press)

37. Herzfeld, K. F. and T. A. Litovitz. Absorption and dispersion of ultrasonic waves. New York, Academic, 1959. 535 p.

38. Herzfeld, K. F. and F. O. Rice. Dispersion and Absorption of high frequency sound waves. The Physical Review 31:691-695. 1928.

39. Hirschfelder, J. O., C. F. Curtiss and R. B. Bird. Molecular theory of gases and liquids. New York, Wiley, 1954. 1219 p.

40. Hocker, L. O., M. A. Kovacs, C. K. Rhodes, G. W. Flynn and A. Javan. Vibrational relaxation measurements in $CO_2$ using an induced-fluorescence technique. Physical Review Letters 17:233-235. 1966.

41. Holmes, R., G. R. Jones and R. Lawrence. Vibrational-rotational-translational energy exchange in some polyatomic molecules. Transactions of the Faraday Society 62:46-53. 1966.

42. Holmes, R., G. R. Jones and N. Pusat. Combined viscothermal and thermal relaxation in polyatomic gases. Transactions of the Faraday Society 60:1220-1229. 1964.

43. _____ Vibrational relaxation in propane, propylene and ethane. The Journal of Chemical Physics 41:2512-2516. 1964.

44. Hooker, W. J. and R. C. Millikan. Shock-tube study of vibrational relaxation in carbon monoxide for the fundamental and first overtone. The Journal of Chemical Physics 38:214-220. 1963.

45. Hudson, G. H., J. C. Mc Coubrey and A. R. Ubbelohde. Energy transfer in polyatomic molecules. I. Catalysis of energy transfer with isotopic molecules. Proceedings of the Royal Society (London), ser. A, 264:289-298. 1961.

46. Hunter, T. F. Degradation of molecular vibrational energy in wall collisions. Journal of the Chemical Society, 1967, p. 1804-1809.

47. Jones, D. G., J. D. Lambert, M. P. Saksena and J. L. Stretton. Rotational and vibrational relaxation in gaseous ammonia. Transactions of the Faraday Society 65:965-973. 1969.

48. Jones, D. G., J. D. Lambert and J. L. Stretton. Vibrational relaxation in mixtures containing oxygen. Proceedings of the Physical Society 86:857-860. 1965.

49. Kauzmann, Walter. Thermal properties of matter. Vol. I. Kinetic theory of gases. New York, Benjamin, 1966. 248 p.

50. Kneser, H. O. Zur Dispersionstheorii des Schalles. Annalen der Physik 11:761-776. 1931.

51. Kovacs, M., D. Ramachandra Rao and A. Javan. Study of diffusion and wall de-excitation probability of $00^{\circ}1$ state in $CO_2$. The Journal of Chemical Physics 48:3339-3341. 1968.

52. Lafferty, W. J., A. G. Maki and E. K. Plyer. High-resolution infrared determination of the structure of carbon suboxide. The Journal of Chemical Physics 40:224-229. 1964.

53. Lambert, J. D. and R. Salter. Ultrasonic dispersion in sulfur dioxide. Proceedings of the Royal Society (London), ser. A, 243:78-83. 1957.

54. _____ Vibrational relaxation in gases. Proceedings of the Royal Society (London), ser. A, 253:277-288. 1959.

55. Lambert, J. D. and E. D. T. Strong. The dimerization of ammonia and amines. Proceedings of the Royal Society (London), ser. A, 200:566-572. 1950.

56. Landau, L. and E. Teller. Zur Theorie der Schalldispersion. Physikalische Zeitschrift der Sowjetunion 10:34-43. 1936.

57. Long, D. A., F. S. Murfin and R. L. Williams. The Raman and infrared spectra of carbon suboxide. Proceedings of the Royal Society (London), ser. A, 223:251-266. 1954.

58. Lord, R. C. and P. Venkaleswarlu. The rotation-vibration spectra of allene and allene-$d_4$. The Journal of Chemical Physics 20:1237-1247. 1952.

59. Lucas, R. and P. Biquard. Nouvelles propriétés optiques des liquides soumis à des ondes ultrasonous. Comptes Rendus Hebdomadaires des Séances de l'Académie des Sciences (Paris) 194:2132-2134. 1932.

60. Lukasik, S. J. Acoustic relaxation by radiation. Journal of the Acoustical Society of America 28:455-458. 1956.

61. Lyot, B. La couronne solaire étudiée en dohors des éclipses. Comptes Rendus Hebdomadaires des Séances de l'Académie des Sciences (Paris) 191:834-837. 1930.

62. McCoubrey, J. C., R. C. Milward and A. R. Ubbelohde. Energy transfer in polyatomic molecules. II. Relative catalytic efficiency for energy transfer to different vibrations to the same molecule. Proceedings of the Royal Society (London), ser. A, 264:299-308. 1961.

63. _____ Transition probabilities for the transfer of vibrational energy. Transactions of the Faraday Society 57: 1472-1481. 1961.

64. Martinez, J. V. Studies of ultrasonic dispersion in gases by the diffraction of light. Ph. D. thesis. Corvallis, Oregon State University, 1962. 167 numb. leaves.

65. Martinez, J. V., J. G. Strauch, Jr. and J. C. Decius. Ultrasonic dispersion observed by optical diffraction. I. Nitrous oxide. The Journal of Chemical Physics 40:186-190. 1964.

66. Meyer, N. J. Multiple vibrational relaxation in gaseous dibromomethane. The Journal of Chemical Physics 33:487-492. 1960.

67. Miller, F. A. and W. G. Fateley. The infrared spectrum of carbon suboxide. Spectrochimica Acta 20:253-266. 1964.

68. Miller, F. A., D. H. Lemmon and R. E. Witkowski. Observation of the lowest bending frequencies of carbon suboxide, dicyanoacetylene, diacetylene and dimethylacetylene. Spectrochimica Acta 21:1709-1716. 1965.

69. Millikan, R. C. Systematics of vibrational relaxation. The Journal of Chemical Physics 39:3209-3213. 1963.

70. _____ Vibrational fluorescence of carbon monoxide. The Journal of Chemical Physics 38:2855-2860. 1963.

71. Millikan, R. C. and L. A. Osburg. Vibrational relaxation of carbon monoxide by ortho- and parahydrogen. The Journal of Chemical Physics 41:2196-2197. 1964.

72. Mills, I. M., W. L. Smith and J. L. Duncan. Coriolis perturbations in the infrared spectrum of allene. Journal of Molecular Spectroscopy 16:349-377. 1965.

73. Moore, C. B. Laser studies of vibrational energy transfer. Accounts of Chemical Research 2:103-109. 1969.

74. _____ Vibration-rotation energy transfer. The Journal of Chemical Physics 43:2979-2986. 1965.

75. Pauling, L. and E. B. Wilson. Introduction to quantum mechanics. New York, McGraw-Hill, 1935. 468 p.

76. Pierce, W. G. Piezoelectric crystal oscillators applied to the precision measurement of the velocity of sound in air and $CO_2$ at high frequencies. Proceedings of the American Academy of Arts and Sciences 60:271-302. 1925.

77. Pitzer, K. S. Quantum chemistry. Englewood Cliffs, Prentice-Hall, 1953. 529 p.

78. Raman, C. V. and N. S. Nagendra Nath. The diffraction of light by high frequency sound waves. Part I. Proceedings of the Indian Academy of Sciences 2:406-412. 1935.

79. _____ The diffraction of light by high frequency sound waves. Part II. Proceedings of the Indian Academy of Sciences 2:413-420. 1935.

80. _____ The diffraction of light by high frequency sound waves. Part III. Proceedings of the Indian Academy of Sciences 3:75-84. 1936.

81. Raman, C. V. and N. S. Nagendra Nath. The diffraction of light by high frequency sound waves. Part IV. Generalized Theory. Proceedings of the Indian Academy of Sciences 3: 119-125. 1936.

82. Rapp, Donald. Complete classical theory of vibrational energy exchange. The Journal of Chemical Physics 32:735-737. 1960.

83. Rapp, Donald and T. Kassal. The theory of vibrational energy transfer between simple molecules in non reactive collisions. Chemical Reviews 69:61-102. 1969.

84. Richards, W. T. Supersonic phenomena. Reviews of Modern Physics 11:36-64. 1939.

85. Rix, H. D. The infrared and Raman spectra of carbon suboxide. The Journal of Chemical Physics 22:429-433. 1954.

86. Ronn, A. M. and D. R. Linde, Jr. Infrared-microwave double resonance using a $CO_2$ laser. The Journal of Chemical Physics 47:3669-3670. 1967.

87. Rossing, T. D. and S. Legvold. Collision excitation of molecular vibrations in halogen-substituted methanes. The Journal of Chemical Physics 23:1118-1125. 1955.

88. Schwartz, R. N. and K. F. Herzfeld. Vibrational relaxation times in gases (three dimensional treatment). The Journal of Chemical Physics 22:767-773. 1954.

89. Schwartz, R. N., Z. I. Slawsky and K. F. Herzfeld. Calculation of vibrational relaxation times in gases. The Journal of Chemical Physics 20:1591-1599. 1952.

90. Secrest, Don and B. R. Johnson. Exact quantum-mechanical calculation of a collinear collision of a particle with a harmonic oscillator. The Journal of Chemical Physics 45:4556-4570. 1966.

91. Sette, D., A. Busala and J. C. Hubbard. Energy transfer by collisions in vapors of chlorinated methanes. The Journal of Chemical Physics 23:787-793. 1955.

92. Sharma, R. D. Deactivation of bending mode of $CO_2$ by hydrogen and deuterium. The Journal of Chemical Physics 50:919-923. 1969.

93. Sharma, R. D. and C. A. Brau. Energy transfer in near-resonant molecular collisions due to long-range forces with application to transfer of vibrational energy from the $\nu_3$ mode of $CO_2$ to $N_2$. The Journal of Chemical Physics 50:924-930. 1969.

94. Shields, F. D. Vibrational relaxation in pure $SO_2$ and $SO_2$/Ar mixtures. The Journal of Chemical Physics 46:1063-1069. 1967.

95. _____ Sound absorption and velocity in $H_2S$ and $CO_2/H_2S$ mixtures. Journal of the Acoustical Society of America 45:481-484. 1969.

96. Shields, F. D. and J. A. Burks. Vibrational relaxation in $CO_2/D_2O$ mixtures. Journal of the Acoustical Society of America 43:510-515. 1968.

97. Solbodskaya, P. V. Determination of the rate of transformation of molecular vibrational energy to translational energy by means of the spectrophone. Isvestia Akademiia Nauk S. S. S. R., Seriia Fizicheskaia 12:656-662. 1948.

98. Stevens, Brian. Collisional activation in gases. Oxford, Pergamon, 1967. 236 p.

99. Strauch, J. G., Jr. Optical diffraction study of ultrasonic sound velocity in nitrous oxide and ammonia gases. Ph. D. thesis. Corvallis, Oregon State University, 1966. 90 numb. leaves.

100. Strauch, J. G., Jr. and J. C. Decius. Ultrasonic dispersion observed by optical diffraction. II. Ammonia. The Journal of Chemical Physics 44:3319-3322. 1966.

101. Stretton, J. L. Calculation of vibrational relaxation times in polyatomic gases. Transactions of the Faraday Society 61: 1053-1067. 1965.

102. Strong, John. Procedures in experimental physics. New York, Prentice-Hall, 1938. 642 p.

103. Tanczos, F. I. Calculation of vibrational relaxation times of the chloromethanes. The Journal of Chemical Physics 25: 439-447. 1956.

104. Taylor, R. L. and S. Bitterman. Experimental measurements of the resonant vibrational energy transfer between mode $\nu_3$ of $CO_2$ and $N_2$. The Journal of Chemical Physics 50:1720-1726. 1969.

105. Torkington, P. Harmonic oscillator contributions to the thermodynamic functions. The Journal of Chemical Physics 18: 1373-1379. 1950.

106. Valley, L. M. and S. Legvold. Sound dispersion in ethane and 1, 1-difluoroethane. The Journal of Chemical Physics 33:627-629. 1960.

107. _____ Sound dispersion in ethane-ethylene mixtures and in halo-ethane gases. The Journal of Chemical Physics 36: 481-485. 1962.

108. Weiss, S. and G. E. Leroi. Direct observation of the infrared torsional spectrum of $C_2H_6$, $CH_3CD_3$ and $C_2D_6$. The Journal of Chemical Physics 48:962-967. 1968.

109. Yardley, J. T. and C. B. Moore. Vibrational energy transfer in methane. The Journal of Chemical Physics 49:1111-1125. 1968.

# APPENDIX

# INTENSITY ASYMMETRY OF FIRST ORDER IMAGES IN ULTRASOUND DIFFRACTION

Intensity asymmetry of first order diffracted light, as indicated in Section (2.3), may be due to one or both of the following:

i) Nonzero incidence between the impinging light rays and the propagating sound waves.

ii) Rapid absorption of the ultrasonic grating.

The generalized theories of light diffraction through ultrasound have been developed for liquids and do not include an absorption term to take into account process (ii) above. Decius (19) has solved the wave equation for light diffraction in an absorbing medium for the special case of zero incidence. His results, stated in equation (68), indicate diffraction asymmetry for the absorbing gas

$$\frac{I(+)}{I(-)} = e^{-4K\sigma} \qquad (\text{when } \beta = 0) \tag{68}$$

where the symbols are as previously defined.

In addition to predicting intensity asymmetry, Decius' development indicates that in regions of rapid acoustic absorption, image blurring of the Lorentz shape will take place. The form of the Lorentz broadening is indicated in equation (84).

$$I_{\pm} \sim \left(\frac{\Lambda n_1}{\lambda}\right)^2 \frac{1}{\left(\sin\theta \pm \frac{\lambda}{\Lambda}\right)^2 + a^2\lambda^2} \tag{84}$$

where the terms have been defined in Section (2. 3).

Since experimental intensity data are not available for gases undergoing vibrational relaxation, a number of gases were selected and the diffraction intensities were recorded. A photomultiplier (RCA Type 1P21) lockin-amplifier assembly was used to measure image intensities. The power supply for the He-Ne gas laser is a Spectra-Physics Model 252 laser exciter which permits up to 50 percent modulation of the output beam. The line shape of the (+1) and (-1) diffraction images was traced photoelectrically by modulating the laser at 20 KHz and scanning over the diffraction pattern with a narrow slit.

Table 8 lists the gases that were studied experimentally along with the necessary parameters for the calculation of the theoretical intensity asymmetry using equation (68). As most gases were scanned at 1 MHz/atm the intensity ratios calculated in Table 8 are also for 1 MHz/atm. The values reported, therefore, do not necessarily represent the maximum diffraction asymmetry observable for the gas. In order to evaluate $\exp(-4\aleph\sigma)$ it was necessary to employ equations (36), (37), (38) and also from Cottrell and McCoubrey (12, p. 17-19) equations (2.46), (2.52), (2.58) and (2.59). Because of the nature of the calculations no attempt was made to employ non-ideality corrections.

The experimental results (not shown) are tentative, due to the

limitations of the scanning method and the difficulties in satisfying the zero incidence restriction. It was readily observable experimentally, however, that as the ratio of $\exp(4K\sigma)$ became progressively larger

i) The intensity asymmetry of the diffracted orders increased.

ii) The image tended to become diffuse and broaden into an oval shape.

iii) The overall signal intensity became much weaker.

Figure 10 shows the first order diffraction images for C Cl $F_3$ over the range 0.2 to 20 MHz/atm. This gas is undergoing dispersion and exhibits an absorption maximum at 1.5 MHz/atm (87). The extent of the broadening can be observed by comparison with the well resolved nitrogen data lying on both sides of the C Cl $F_3$ sequence. The intensity asymmetry between the (+1) and (-1) diffraction orders may be seen on the original photographic plate, but is not well represented in Figure 10 due to the difficulties associated with the copying process.

The theoretical asymmetry intensities for C Cl $F_3$ at the (f/p) values listed in Figure 10 are listed below:

| (f/p) | 0.2 | 0.6 | 2.0 | 6.0 | 2.0 |
|---|---|---|---|---|---|
| $\exp(-4K\sigma)$ | 1.29 | 1.90 | 2.24 | 1.44 | 1.14 |

At frequencies above 10 MHz/atm the classical contribution to the

absorption coefficient becomes important and this term has been included in the calculations. If it were possible to make very accurate measurements of the intensity ratio, $\frac{I(+)}{I(-)}$, this method could be used to measure vibrational relaxation times in gases.

Unfortunately, the diffraction asymmetry theoretically predicted for an absorbing gas is obscured by the asymmetry which results when the zero incidence condition is not satisfied. David's theory for nonabsorbing gases, developed in Section (2.3), gives the intensity asymmetry as a function of the angle, $\beta$, between the impinging light rays and the sound wave front.

$$\frac{I(+)}{I(-)} = \left[\frac{(\bar{\beta} - 1/2)\sin(\bar{\beta} + 1/2)\sigma}{(\bar{\beta} + 1/2)\sin(\bar{\beta} - 1/2)\sigma}\right] \qquad (63)$$

where

$$\bar{\beta} = \frac{\Lambda}{\lambda}\beta$$

Using equation (63) we see that the ratio of $\frac{I(+)}{I(-)}$ is unity at normal incidence in nonabsorbing media. At the Bragg angle, when the asymmetry is at a maximum, equation (63) reduces to the following expression.

$$\frac{I(+)}{I(-)} = \left(\frac{\sigma}{\sin\sigma}\right)^2 \qquad \text{when} = -\frac{\lambda}{2\Lambda} \qquad (66)$$

As the acoustic wavelength becomes smaller (e.g., by examining gases of progressively lower sound velocities) equation (66) indicates

that the maximum intensity asymmetry observed should be getting larger. This progressive pattern is similar to that predicted for absorbing gases as can be noted from Table 8. The intensity asymmetries which have been experimentally observed could, therefore, be ascribed to a failure to meet the zero incidence requirement. The Bragg angle is very small and varies from one to three milliradians.

The great limitation of David's theory is that it is not applicable in the region of interest and intensity ratios cannot justifiably be calculated. The limiting inequality imposed on David's theory is shown in equation (64).

$$\frac{\pi \lambda d}{2\Lambda^2} = \frac{\sigma}{2} << 1 \qquad (64)$$

The gas listed in Table 8 which comes closest to satisfying this restraint is $C_2H_4$ where $(\sigma/2) = 0.36$ (at 1 MHz/atm) and, using equation (66), $\frac{I(+)}{I(-)} = 1.2$. The theory is not at all applicable to C Cl $F_3$ where $(\sigma/2) = 1.42$; but for comparison, $\frac{I(+)}{I(-)} = 90$.

The sensitivity of the (+1) and (-1) diffraction orders to departure from zero incidence has been demonstrated experimentally. Figure 11 reveals the intensity asymmetry which occurs in C Cl $F_3$ (at 0.6 MHz/atm) as the angle between the light rays and the sound wave front is varied. It should be noted that the scale showing angle tilt does not indicate at zero radians the condition of

normal incidence. This position refers to the cell setting for the $C\,Cl\,F_3$ sequence shown in Figure 10.

The experimental method employed in this preliminary study proved to be insufficient to distinguish between diffraction asymmetry arising from acoustic absorption and from non-zero incidence of the light beam and sound waves. Using the proper instrumentation it should be possible to test the validity of equation (68) which was derived by Decius for zero incidence and an absorbing gas. Also it would be significant to extend Decius' results to take into account the angle effect on the diffraction asymmetry. Finally, the method should be explored to determine if meaniful relaxation parameters could be determined from intensity data.

Table 8. Diffraction asymmetry at one MHz/atm in gases undergoing vibrational relaxation.

| Gas | $\tau(\mu \text{ sec})^*$ | $V_o^2 \times 10^4 m^2/sec^2$ | $V_\infty^2 \times 10^4 m^2/sec^2$ | $\kappa \times 10^{-2}$ | $\sigma$ | $e^{4\kappa\sigma}(I+/I-)$ |
|---|---|---|---|---|---|---|
| OCS | 1.6 | 5.189 | 5.812 | 1.7 | 1.50 | 1.11 |
| $C_2H_4$ | 0.22 | 10.979 | 11.857 | 4.0 | 0.73 | 1.12 |
| $BF_3$ | 0.090 | 4.401 | 4.904 | 3.3 | 1.80 | 1.27 |
| $CF_4$ | 0.76 | 3.279 | 3.779 | 5.0 | 2.32 | 1.59 |
| $CCl_2F_2$ | 0.078 | 2.330 | 2.750 | 3.7 | 3.40 | 1.65 |
| $CClF_3$ | 0.24 | 2.725 | 3.184 | 7.5 | 2.84 | 2.34 |
| $CBrF_3$ | 0.20 | 1.900 | 2.233 | 6.4 | 4.06 | 2.86 |
| $SF_6$ | 0.78 | 1.866 | 2.277 | 9.2 | 4.04 | 4.53 |

*Vibrational relaxation times are from Cottrell and McCoubrey (12, p. 77-122).

Figure 11. Intensity asymmetry in the first order diffraction images in $C Cl F_3$ when the zero incidence condition is not fulfilled.

Best scan available. Original is dark.